TITLE PAGE

A *P2RX7* single nucleotide polymorphism haplotype promotes exon 7 and 8 skipping, which is predicted to disrupt the P2X7 receptor ATP-binding site

Kristen K. Skarratt[1], Ben J. Gu[2], Michael D. Lovelace[1], Carol J. Milligan[2], Leanne Stokes[1,3], Rachel Glover[1], Steven Petrou[2], James S. Wiley[2], and Stephen J. Fuller[1]

[1]The University of Sydney, Department of Medicine, Faculty of Medicine and Health, Nepean Clinical School, Kingswood, NSW 2747 Australia

[2]Florey Neurosciences Institute, University of Melbourne, VIC 3010 Australia

[3]School of Pharmacy, University of East Anglia, Norwich Research Park, Norwich, United Kingdom

*Running title: *Inheritance of alternative splicing for the P2X7 receptor*

To whom correspondence should be addressed: Stephen J Fuller, Nepean Clinical School, The University of Sydney, 62 Derby Street, Kingswood, NSW, 2747, Australia

Tel.: +61 2 47343732; Fax: +61 2 47341817; E-mail: stephen.fuller@sydney.edu.au

Nonstandard Abbreviations

Anti-EE	polyclonal rabbit anti–glutamic acid-glutamic acid antibody
BS3	bis(sulfosuccinimidyl) suberate
DTSSP	3,3'-dithiobis(sulfosuccinimidyl propionate)
LD	linkage disequilibrium
OBB	Odyssey blocking buffer
PI	protease inhibitor cocktail
PLA	proximity ligation assay
TM	transmembrane domain

ABSTRACT

P2X7 is an ATP-gated membrane ion channel that is expressed by multiple cell types. Brief exposure to ATP induces the opening of a non-selective cation channel; while repeated or prolonged exposure induces formation of a transmembrane pore. This process may be partially regulated by alternative splicing of full-length *P2RX7A* pre-mRNA, producing isoforms that delete or retain functional domains. Here we report cloning and expression of a novel *P2RX7* splice variant, *P2RX7L,* that is characterized by skipping of exons 7 and 8. In HEK 293 cells, expression of *P2RX7L* produces a protein isoform, P2X7L, that forms a heteromer with P2X7A. A haplotype defined by 6 single nucleotide polymorphisms (rs208307, rs208306, rs36144485, rs208308, rs208309 and rs375655596) promotes allele-specific alternative splicing, increasing mRNA levels of *P2RX7L* and another isoform, *P2RX7E,* which in addition has a truncated C-terminus. Skipping of exons 7 and 8 is predicted to delete critical amino acids in the ATP-binding site. P2X7L-transfected HEK 293 cells have phagocytic but not channel or pore function, and double-transfected P2X7L and P2X7A cells have reduced pore function. Heteromeric receptor complexes of P2X7A and P2X7L are predicted to have reduced numbers of ATP-binding sites, which potentially alters receptor function compared to homomeric P2X7A complexes.

Keywords: P2X7, alternative splicing, heteromer, single nucleotide polymorphism

INTRODUCTION

The P2X family contains seven ATP-gated surface membrane receptors (P2X1–P2X7) that form functionally distinct homomeric and/or heteromeric ion channels (1). The P2X7 receptor is expressed on cells throughout the human body, including the immune and neurological systems, and is implicated in a wide range of physiological processes (2). P2X7 activation by ATP is a physiological stimulus for the release of interleukin-1β, and proteolytic cleavage of soluble IL-6 receptor, matrix metalloproteinase-9, CD62L, and CD23 (3-5). Brief exposure to extracellular ATP, released from cellular sources in response to cell stress and tissue damage, induces opening of a non-selective cation channel; while repeated or prolonged application of ATP results in the formation of a transmembrane pore (6), and ultimately results in cell apoptosis via caspase activation (7). In addition, P2X7 functions as a macrophage scavenger receptor, however in contrast to channel and pore functions, phagocytic function is inhibited by ATP (8, 9).

The mechanism by which P2X7 transitions from ion channel to pore in response to the same ligand has not been fully elucidated. However, *in vitro* studies using wild-type and non-dilating mutant rat P2X7 support partial to full occupancy of ATP-binding sites as a determinant of transition from desensitized states to sensitized/dilated states respectively (10). Furthermore, concentration-dependent saturation of ATP-binding sites may explain opposing P2X7-dependent functions observed in human T cell subsets (11).

ATP binding sites are located between each of the three P2X7 protein subunits that form the cation-selective channel (12). For each of the subunits, the location of conserved amino acid residues required for ATP binding can be inferred from the agonist-bound crystal structure of zP2X4 (13). Within the first subunit, the ammonium groups of lysine 64 and lysine 66, encoded by exon 2 of the P2X7 gene, *P2RX7,* are predicted to form hydrogen bonds with ATP phosphate groups. In the second subunit, ATP interacts with asparagine 292 and arginine 294, encoded by exon 8, and lysine 311, encoded by exon 9 (14, 15). P2X7 function can be significantly affected by inheritance of an exon 9 single nucleotide polymorphism (SNP) rs28360457 (Arg307Gln) that abolishes P2X7-dependent channel and pore function in human B lymphocytes and peripheral blood mononuclear cells (PBMCs) (16).

Alternative splicing of genes produces a variety of alternatively spliced messenger RNAs (mRNAs) that encode distinct proteins (17), and to date, 11 alternatively spliced isoforms of *P2RX7* have been identified (18-21). However, only 2 of these, *P2RX7B* and *P2RX7E,* are predicted to be translated to proteins containing the topological features that define members of the P2X receptor family, consisting of two transmembrane domains, an extracellular loop and intracellular amino and carboxy termini (22). *P2RX7B* gives rise to a protein with a truncated intracellular C-terminus that retains the ATP-binding sites in the extracellular domain, and potentiates channel and pore function when co-expressed with full-length *P2RX7A* (19). *P2RX7E* is identical to *P2RX7B* except that exons 7 and 8, which encode part of the ATP-binding site in the extracellular domain, are also deleted (18).

There is considerable inter-individual variation in P2X7 function that results from inheritance of nonsynonymous DNA sequence variations (23, 24); however a proportion of this variation may result from alternative splicing. The aim of the present study was to study inter-individual differences in *P2RX7* alternatively spliced isoform expression, in particular

mRNAs that lack exons 7 and 8 (EX7_EX8del mRNA) and within this group identify novel mRNA and protein isoforms that alter receptor function. Furthermore, we aimed to determine if the expression of alternatively spliced variants was heritable.

MATERIALS AND METHODS

Cell Isolation, RNA and DNA extraction

The experimental protocol was approved by the Nepean and Blue Mountains Local Health District Human Research Ethics Committee (06/58). Peripheral blood samples were collected from 24 subjects after obtaining informed consent. PBMCs were isolated from whole blood using density gradient centrifugation over Ficoll-Paque™ (GE Healthcare, Chicago, IL, USA). Isolated cells were preserved at -80°C in RNAprotect (Qiagen, Hilden, NW, Germany) until RNA extraction was performed using Tri-Reagent (Sigma-Aldrich, St. Louis, MO, USA) according to the manufacturer's protocol, using 1-bromo-3-chloropropane as an alternative to chloroform. Reverse transcription was performed at 42°C for 30 min using a Tetro cDNA Synthesis kit (Bioline, Taunton, MA, USA) and a 1:1 ratio of oligo dT and random hexamers unless stated otherwise. DNA was isolated from whole blood using a Wizard DNA Extraction kit (Promega, Madison, WI, USA). Sequencing and SNP genotyping were performed at the Australian Genome Research Facility (AGRF, St Lucia, QLD, Australia).

Reverse transcription PCR

Reverse transcription PCR (RT-PCR) was performed using a Rotor-Gene 2000 cycler (Corbett Life Science; Qiagen) under the following cycling conditions: 95°C for 10 min; then 45 cycles of 95°C for 15 s, 55°C for 15 s, 72°C for 15 s followed by a melt curve beginning at 72°C for 45 s and increasing to 95°C in increments of 1°C, holding for 5 s at each temperature. Each reaction was performed in a volume of 10 µl containing up to 1 µl cDNA, Sensimix Sybr No Rox Mastermix (Bioline) and 750 nM of appropriate forward and reverse primer (Optimal primer concentrations were determined in preliminary experiments, data not shown). For qualitative assessment of *P2RX7* isoform profiles, single reactions were performed as described above using primer sets 1-3 (Table 1). Products were separated by electrophoresis on a 2% agarose gel containing Sybrsafe DNA stain (Thermo Fisher Scientific, Waltham, MA, USA) and visualized on a GelDoc system (Bio-Rad Laboratories, Hercules, CA, USA). Primer sets 4-9 (Table 1) were used for quantitative RT-PCR (qRT-PCR) and each reaction was performed in triplicate as described above. Expression of each subgroup (amplified by primer sets 5-9, Table 1) was measured relative to total *P2RX7* expression (amplified by primer set 4, Table 1). No-template controls and normalization controls using *GAPDH* primers were included in each run.

To determine transfection ratios of plasmid RNAs in double-transfected HEK 293 cells, cDNA synthesis was performed using oligo(dT)-priming and RT-PCR was performed using Set 4 and Set 9 which detect mRNA transcribed from plasmids P2X7A or P2X7L and P2X7E or P2X7L respectively. P2X7E mRNA derived from the plasmid is truncated in intron 10, unlike naturally occurring P2X7E mRNA, and is not detected by Set 4 primers in RNA from transfected cells. Fold expression above GAPDH was calculated using the following formula: Fold expression = $1/[2\ Ct_{(Set\ 4\ or\ 9)} - Ct_{(GAPDH)}]$.

Cloning

PolyA tailed mRNA was reverse transcribed using a Tetro cDNA synthesis kit (Bioline) as described by the manufacturer at 42°C for 60 min. *P2RX7* specific sequences were amplified from cDNA using previously described primers (21) and Phusion Hotstart II High Fidelity polymerase (Finnzymes; Thermo Fisher Scientific) with the following

cycling parameters: 98°C for 30 s followed by 34 cycles at 98°C for 10 s, 72°C for 60 s, then 72°C for 5 min, followed by cloning into a pGemTeasy vector (Promega) according to the manufacturer's instructions except that heat shock was performed in a heat block rather than a water bath. Colony screening was performed using qRT-PCR to identify specific isoform clones as previously described using primer sets 4-9 (Table 1) (25).

For subcloning into the pcDNA3.1 expression vector, a HindIII site was added to the 5' end and a GluGlu (EE) Tag and XbaI site were added to the 3'end of *P2RX7E* and *P2RX7L* fragments using a common forward primer: 5'-ggg**aagctt**tcaccatgccggcctgctgc-3'; and for *P2RX7E* reverse primer: 5'-ccc**tctaga**ctcgagctattccattggcatgtattcgtttaaacc***gtcacttccttctccaaaccatttt*-3'**and for *P2RX7L* reverse primer: 5'-ccc**tctaga**ctcgagctattccattggcatgtattcgtttaaacc***gtaaggactcttgaagccactgta*-3'** (restriction sites in bold; EE tag sequence underlined and *P2RX7* specific sequence italicised) by amplification using Phusion HotStart II as described above. After double digestion with HindIII and Xba1 (NEB, Ipswich, MA, USA) and gel purification using an Illustra GFX PCR and Gelband Purification Kit (GE Healthcare), amplified fragments were ligated into pcDNA3.1 using T4 ligase and transformed into JM109 cells (Promega) according to the manufacturer's instructions. Plasmids were purified from clones of interest using a MiniPrep Plasmid extraction kit (Promega) and sequenced to confirm cloning of the correct *P2RX7* isoform sequence.

Cell lines

HEK 293 cells were maintained in DMEM: F12 medium containing 10% fetal calf serum, 2 mM L-glutamine, 100 U/ml penicillin, and 100 μg/ml streptomycin (all from Invitrogen, Carlsbad, CA, USA) at 37ºC with 5% CO_2 in a humidified incubator. PJB3 and *P2RX7A*-His are cell lines derived from HEK 293, stably transfected with *P2RX7A* c-terminal labelled with a Glu-Glu (EE) or His tag, respectively.

Plasmid DNA (1 μg, unless stated otherwise) was transiently transfected into HEK 293 cells (35 mm petri dish of near confluent cells) using Lipofectamine 2000 (3 μl/200 μl of Optimem, Invitrogen). Transfected cells were harvested after 24-48 hr or subjected to Geneticin selection (400 μg/ml) (Gibco; Thermo Fisher Scientific) to generate stably transfected cell lines.

Exon trapping

DNA sequences spanning *P2RX7* exon 7 and flanking intronic sequences were amplified from 2 subjects (one wild-type and one homozygous minor allele at rs208307) with the addition of BamH1 and Not 1 restriction sites using the following primers: left 5'-acgtaaggatcctgggatttgacgaggtatgg-3' and right 5'- acgtaagcggccgcccatatgccattggtcacac -3', and recombinant Pfu DNA polymerase (Thermo Fisher Scientific) according to the manufacturer's standard protocol. The amplified fragments were ligated into linearized pSPL3 vectors (a kind donation from Dr Robert Formosa, DNA Laboratory, Faculty of Health Sciences, University of Malta, Malta) with T4 ligase and transformed into HB101 competent cells (Promega) as described by the manufacturer. Purified plasmids were transfected into HEK 293 cells and harvested for RNA extraction as described above. cDNA synthesis was performed as described above using only oligo dT

priming and then PCR was performed as previously described (26) using an annealing temperature of 58°C and pSPL3 specific primers (SD6: 5'-tctgagtcacctggacaacc-3'; SA2: 5'-atctcagtggtatttgtgagc-3').

***In vitro* electrophysiology measurements**

HEK 293 cells were transiently transfected with empty vector, *P2RX7A*, *P2RX7E* or *P2RX7L* constructs. Post-transfection (48 hr), cells were detached using 0.5 mL Accutase® Cell Detachment Solution (Innovative Cell Technologies Inc., San Diego, CA, USA) and resuspended at a density of 1 x 10^6 – 5 x 10^7 cells/mL in 50% serum-free media and 50% external recording solution v/v. The external recording solution comprised 145 mM NaCl, 5 mM KCl, 1 mM $MgCl_2$, 2 mM $CaCl_2$, 13 mM D-glucose, and 10 mM HEPES (pH 7.4 with NaOH; ~298 mOsm). The internal recording solution comprised 85 mM NaCl, 60 mM NaF, 10 mM EGTA, and 10 mM HEPES (pH 7.2 with NaOH; ~285 mOsm). Solutions were filtered using a 0.2 μm membrane filter (Minisart; Sartorius Stedim Biotech, Goettingen, Germany). Cells were kept in suspension by gentle automatic pipetting. Currents generated by P2X7 were recorded using a NPC-16 Patchliner® (Nanion Technologies GmbH, Munich, Germany) patch-clamp instrument in the whole-cell configuration. Medium single-hole planar NPC-16 chips with an average resistance of ~2.5 MΩ were used. Pipette and whole-cell capacitance were fully compensated. Recordings were acquired at 1 kHz with the low pass filter set to 0.33 kHz in PATCHMASTER (HEKA Instruments Inc., NY, USA) and performed at room temperature. P2X7 receptor-dependent currents were induced by application of 1 mM ATP. The cells were held at -50 mV. Offline analysis was performed using MATLAB R2015a (The Math Works Inc., Natick, Massachusetts, United States) and GraphPad Prism 6 (Molecular Devices). Data are shown as means ± standard error of the mean (SEM). Statistical analysis was performed using Student's *t*-test. Statistical differences were considered significant when $p < 0.05$.

Calcium flux measurements

Transfected HEK 293 cells (~2 x 10^6/mL) were washed once and loaded with 2 μM Fura-Red acetoxymethyl ester by incubation at 37°C for 30 min in Ca^{2+} free HEPES buffered NaCl medium. Cells were washed once and incubated in HEPES buffered NaCl with 1 mM Ca^{2+} for another 30 min. HEK 293 cells were then washed twice and resuspended in 3 mL HEPES buffered KCl medium at a concentration of 2 x 10^6/mL. Samples were stirred at 37°C and stimulated with 1 mM ATP after addition of 3.0 mM $CaCl_2$. Cells were analysed by a Becton Dickinson FACSCalibur flow cytometer at acquisition rates of ~2000 events/s. The kinetic linear mean channel of fluorescence intensity (1024 channels resolution) for each gated subpopulation over successive 2 s intervals was plotted against time and saved into a text file as described previously (27).

Phagocytosis measurements

Transfected HEK 293 cells (~2 x 10^6/mL) were resuspended in HEPES-buffered NaCl medium (145 mM NaCl, 5 mM KCl, 10 mM HEPES, pH 7.5, plus 5 mM D-glucose, 0.1% BSA, and 0.1 mM $CaCl_2$). For phagocytosis assay, 1.0 μm (5 μL) carboxylated yellow-green (YG) beads (Polyscience, USA) were added at zero time. The linear mean channel of fluorescence intensity for gated HEK 293 cells over successive 10 s intervals was analysed by WinMDI software and plotted against time, as described previously (28). Student's *t*-test was used to assess differences between mutant and wild-type constructs.

Ethidium bromide uptake measurements.

P2X7 pore function in transfected HEK 293 cells was assessed by ATP stimulated ethidium$^+$ uptake as previously described using either a plate reader based assay (29) or by time resolved flow cytometry (30). Briefly, cells were bathed in a low divalent medium containing ethidium bromide (25 μM) and opening of the P2X7 pore was stimulated by the addition of 1 mM ATP allowing passage of ethidium$^+$ into the cell. The increase in fluorescence signal as the ethidium$^+$ binds to DNA was monitored over time.

Preparation of whole-cell lysates

Cells were placed on ice and washed 3 times with cold phosphate buffered saline (PBS) and harvested by scraping in the presence of 0.5 ml PBS with mini-Complete Protease Inhibitor cocktail EDTA-free (PI, Roche Holding AG, Basel, Switzerland). Pelleted cells were lysed with 50 μl TX-100 lysis buffer (20 mM Tris pH7.4, 100 mM NaCl, 1% Triton-X-100) plus PI. After 30 min on ice, whole-cell lysates were harvested by centrifugation (14,000 x g, 10 min at 4°C).

Western blotting

Equal amounts of protein were heated at 70°C for 10 min in NuPAGE® loading buffer (Invitrogen) +/- 5mM Dithiothreitol (DTT). Samples and markers (Hyperpage, or Novex Sharp Protein Standard, Invitrogen) were separated on NuPAGE® Novex 4-12% Bis-Tris mini gel in a XCell SureLock mini-Cell system with NuPAGE® MOPS SDS Running Buffer (all from Invitrogen) by running at 60 V for 30 min followed by 120 V for 120 min or Tris-Acetate mini gels with NuPAGE® Tris-Acetate SDS Running Buffer as indicated. Proteins were transferred to a PVDF membrane (Thermo Fisher Scientific) using an XCell II Blot Module (Bio-Rad laboratories, Hercules CA, USA; 350 mA for 50 min) in NuPAGE® Transfer Buffer (Invitrogen).

After blocking for 2 hr or overnight with non-animal protein (NAP)-blocker (G-Biosciences, St. Louis, MO, USA) and washing 3 times in 0.5% Tween20 in Tris-Buffered Saline (TBS) for 10 min with shaking, the membrane was incubated with primary antibodies (polyclonal rabbit anti–Glu-Glu antibody, Bethyl Laboratories, Montgomery, TX, USA, 1:10,000) or extracellular P2X7 antibody, APR-008, (anti P2X7, Alomone Labs, Jerusalem, Israel; 1:5,000) for 2 hours, washed again as above and probed with goat anti-rabbit horseradish peroxidase (Santa Cruz Biotechnology, Dallas, TX, USA, 1:10000) for 1 hr. After further washing, bands were visualized using a SuperSignal West Pico or Femto kit (Thermo Fisher Scientific) on a Gel Doc System (Bio-Rad).

For near infrared immunoblotting, proteins were transferred to Immobilon-FL membranes (Merck Millipore, Tullagreen, Ireland) by overnight transfer at 30 V. Membranes were rinsed with water and dried for 1 hr before re-wetting and blocking for 1 hr in Odyssey Blocking Buffer (OBB, Licor, Lincoln, NB, USA) prepared in TBS as described by the manufacturer. Primary antibodies were used as described above; except they were prepared in OBB plus 0.1% Tween 20. Washes were performed as above, but with 0.1% TBS. Blots were incubated with secondary antibody (800CW Donkey anti-Rabbit IgG, Licor) diluted 1:20000 in OBB plus 0.1% Tween 20 plus 100 μg/ml sodium dodecyl sulfate for 1 hr in the dark. The blots were washed 4 times, rinsed in TBS and air dried in the dark. Images were collected on an Odyssey Fc Imager (Licor).

Immunofluorescent Staining for Flow cytometry

Transfected HEK 293 cells were stained either directly with anti-P2X7 monoclonal antibody (mAb) L4-FITC (1:200), or indirectly with anti-P2X7 (1:40) and goat anti rabbit IgG-FITC (Santa Cruz Biotechnology,1:200) and analysed using a FACSVERSE flow cytometer (BD Biosciences, Franklin Lakes, NJ, USA).

Crosslinking of Cell Surface Receptors

All crosslinking was performed on cells attached to culture flasks. To crosslink surface receptors with Bis[sulfosuccinimidyl]suberate (BS3, Thermo Fisher Scientific), cells were washed 3 times with cold PBS (pH 8) and incubated with 1.25 mM BS3 for 30 min at RT. The reaction was quenched by addition of 20 mM Tris HCl (pH 7.5) followed by incubation at room temperature for 15 min. Cells were harvested for western blotting as described above. Crosslinking with 0.5 mM 3,3'-dithiobis(sulfosuccinimidyl propionate) (DTSSP, Thermo Fisher Scientific) was performed as above except that PBS (pH 7.4) was used.

Proximity Ligation Assay

Dishes (35 mm) of subconfluent HEK 293 cells stably transfected with EE-labelled *P2RX7A* or *P2RX7L* were transiently transfected with 0.25 µg of *P2RX7A*-AcGFP plasmid. After 24 hrs, cells were trypsinized and a 1/5 dilution replated onto poly-D-Lysine coated coverslips in a 24 well plate. After a further 24 hrs, cells were fixed by washing once with cold PBS, then incubating for 20 min on ice with 4% paraformaldehyde in PBS. Fixed cells on coverslips were washed twice with PBS and permeabilised with 0.5% Triton X-100 in PBS for 10 min at RT, then blocked for 30 min at RT in 5% FCS in PBS.

Coverslips were incubated overnight at 4˚C with rabbit anti-EE (1/800) and mouse anti-GFP antibody (1/800, Santa Cruz Biotechnology). Coverslips were then attached to slides with Twinsil (Picodent, Wipperfürth, NW, Germany), cell-side-up before proceeding with the proximity ligation assay (PLA) using a Duolink® In Situ Orange mouse/rabbit starter kit (Sigma-Aldrich, St Louis, MO, USA) according to the manufacturer's instructions. Signals were observed with an Eclipse 80i fluorescent microscope with a 40x objective using B2A, G2A and UV-2A filter sets (Nikon Instruments, Melville, NY, USA) to detect AcGFP, PLA and DAPI signals, respectively. Images were collected with a Qicam Fast1394 camera (Qimaging, Surrey, BC, Canada) using a constant, optimised exposure time for collection of all images.

Nickel affinity chromatography

Pull-down of His-tagged proteins was performed using EZview™ Red HIS-Select® HC Nickel Affinity beads as described by the manufacturer (Sigma- Aldrich). Briefly, whole-cell lysates (~1 µg protein) were incubated with pre-equilibrated beads in the presence of 10 mM or 12.5 mM Imidazole in PBS plus 1% Tx-100 plus PI, for 2 hr at 4ºC with slow rotation, then washed 4 times with the same buffer. Proteins were eluted from the washed pellet in 15 µl of NuPAGE loading buffer (Invitrogen) with or without 5 mM DTT as required.

Statistical analyses

Fishers' exact tests were performed using an online tool (www.quantpsy.org/fisher/fisher.html) and one-way ANOVA with Tukey's post hoc analyses were performed in GraphPad Prism v7. Pairwise linkage disequilibrium (LD) was calculated using PLINK (http://pngu.mgh.harvard.edu/purcell/plink/) (31).

RESULTS

Expression patterns of *P2RX7* mRNA isoforms vary between human subjects

PBMCs from 22 human subjects were used to qualitatively determine inter-individual differences in expression of *P2RX7* mRNA isoforms. PCR primers (Sets 1-3, Table 1A) were designed to span known alternatively spliced regions of the *P2RX7* primary mRNA transcript. Each set of primers generated amplicons of different sizes, depending on the isoforms present in the sample which, when assessed by Southern blot, enabled a qualitative analysis of *P2RX7* isoform expression. The predicted banding patterns in the presence of all known *P2RX7* isoforms are represented schematically in Fig. 1A (left panel) alongside 2 examples of typical isoform expression patterns seen in individuals (Fig. 1A, central and right panels). Reduced complexity of banding patterns in individuals compared to the predicted patterns indicated that a subset of *P2RX7* mRNA isoforms are normally expressed and in varying abundances. In subject 1, absence of a 130 base pair (bp) band generated by primer set 1 excluded the presence of *P2RX7V7*, *P2RX7ΔE2* and *P2RX7V4*; absence of 385 and 35 bp bands from Set 2 excluded the presence of *P2RX7D,* and absence of a 199 bp band from Set 3 excluded *P2RX7E*. Weak detection of a 438 bp band generated by Set 1 and a 159 bp band generated by Set 2 indicated low levels of isoforms *P2RX7G* and *H,* and *P2X7C* and *F*, respectively. From these data it was inferred that of 12 known *P2RX7* isoforms, subject 1 predominantly expressed isoforms *P2RX7A*, *P2RX7B* and *P2RX7J* as well as small amounts of isoforms *P2RX7C, F, G* and/or *H*. Of interest was the inter-individual differences in the presence of the 199 bp band detected by Set 3 (Fig. 1A, arrow) representing Ex7_Ex8del mRNAs, which was absent in 10 of 22 subjects tested.

P2RX7 mRNA isoforms can be grouped on the basis of specific exon deletions or insertions (18). A set of 6 primers were designed to enable relative quantification of each isoform sub-group as a percentage of total *P2RX7* mRNA in 24 subjects (Table 1B, primer sets 4-9, and Fig. 1B). In PBMCs, the inserted intron 10 (Ins Int 10) mRNA group (containing *P2RX7B*, *P2RX7C*, *P2RX7E*, *P2RX7G*, *P2RX7V4* and *P2RX7V7*) was the most abundant in each individual (mean = 60.7% ± 12.2 SD), followed by deletion Exon 4 (*P2RX7C* and *P2RX7F;* mean = 10.4% ± 4.8 SD), and deletion Exon 8 (*P2RX7J*, *P2RX7F* and *P2RX7V4*; mean = 5.9% ± 3.0 SD). Ins N3 variants (*P2RX7G* and *P2RX7H*) were consistently least abundant (Fig. 1B; mean = 0.5% ± 0.7 SD). Levels of Ex7_Ex8del mRNA (*P2RX7E*) were detected at levels ranging from 0-13% of total *P2RX7* (mean = 3.2% ± 3.4 SD), consistent with qualitative analyses.

Isolation of a novel EX7_EX8del mRNA variant

To investigate whether inter-individual variation in EX7_EX8del mRNA variants was due to *P2RX7E* levels alone or the presence of other variants, *P2RX7E* mRNA was cloned from 2 subjects that expressed high levels of EX7_EX8del mRNA. Colony screening was performed using primer sets 4-9 (Table 1B) to identify clones of specific isoforms as previously described (25). In addition to isolating *P2XR7E* mRNA, 5 novel *P2RX7* mRNA variants were identified (Fig. S1). Of interest was a novel EX7_EX8del mRNA isoform designated "*P2RX7L*" (Fig. 2A and S1; GenBank accession, MK465687) that was predicted to be translated into a 506 amino acid (aa) protein retaining the long intracellular C-terminus of P2X7A (Fig. 2B and S2).

EX7_EX8del mRNA levels are associated with an intron 6 SNP, rs208307

From our SNP genotyping database, we identified four *P2RX7* SNPs that were predicted to influence exon 7 and 8 skipping: rs208307 (acceptor splice site in intron 6), rs503720 (upstream of the intron 7/exon 8 junction), rs7958311 (exon 8 missense mutation), and rs7958316 (exon 8 missense mutation at an exonic splice enhancer site). Allele frequencies of these SNPs were compared between subjects that expressed EX7_EX8del mRNA (Table 2). The minor allele frequency (MAF) of rs7958311 was significantly higher in EX7_EX8del negative subjects (MAF = 0.5) compared to positive subjects (MAF = 0.15; n = 17; $p = 0.02$). Conversely the MAF for rs208307 was 0 for EX7_EX8del negative subjects compared to 0.43 for EX7_EX8del positive subjects ($p = 0.007$). No associations were found between EX7_EX8del mRNA levels and the other two SNPs (rs503720 and rs7958316).

Amongst the EX7_EX8del positive subjects, the lowest level of expression was seen in subjects wild-type at rs208307. To determine if EX7_EX8del mRNA levels were associated with gene-dosage of rs208307 we analysed EX7_EX8del mRNA levels as a percentage of total *P2RX7* mRNA in wild-type (CC), homozygote minor allele (GG) and heterozygote (CG) subjects and found a difference between the three groups (one-way ANOVA $p < 0.0001$ followed by Tukey's post hoc analysis). Expression of EX7_EX8del mRNA was highest in subjects homozygous for the minor allele (P2X7L mean expression = 9.1% ± 4.5 SD), intermediate in heterozygote (mean = 5.0% ± 1.8 SD) and lowest in wild-type participants (mean = 0.5% ± 1 SD, Fig. 3A). Gene dosage of rs7958311 was not associated with levels of EX7_EX8del mRNA (data not shown).

A SNP haplotype block tagged by rs208307 regulates EX7_EX8del mRNA levels

The rs208307 SNP is located 5 bp from the intron 6/exon 7 boundary, and is predicted to disrupt a branch-point site associated with exon splicing [Human Splice Finder 2.4.1 software (HSF), http://www.umd.be/HSF/] (32). An exon-trapping system was used to study the effect of rs208307 wild-type (CC) and homozygous minor allele (GG) on *P2RX7* splicing (Fig. 3B). A 494 bp DNA fragment encompassing *P2RX7* exon 7 and flanking intronic sequences was cloned from one wild-type (CC) subject and one homozygous minor allele (GG) subject and inserted into a pSPL3 exon trapping vector. HEK 293 cells were transiently transfected with either CC, GG or empty trapping vectors. RT-PCR was performed on extracted RNA using plasmid specific primers SD6 and SA2. Cells transfected with plasmid derived from the wild-type subject, produced a 393 bp band (Fig. 3C), which was confirmed by sequencing to contain *P2RX7* exon 7. The plasmid derived from the homozygous minor allele subject generated 2 fragments, a 393 bp amplicon containing *P2RX7* exon 7, as well as a 263 bp amplicon confirmed by sequencing to contain only Exon 1 and Exon 2 of pSPL3, consistent with partial exon 7 skipping (Fig. 3C).

Sequencing of the 494 bp fragments inserted into the exon trapping plasmid identified additional SNPs surrounding rs208307 that were subsequently analysed *in silico* for their effect on alternative splicing (HSF and RegRNA software, http://regrna2.mbc.nctu.edu.tw/) (32, 33). The rs208307 homozygous minor allele subject was homozygous for minor alleles at rs208306, rs36144485 (both in intron 6), and rs208308, rs208309, and rs373655596 (all in intron 7). *In silico* analysis predicted that rs208306 SNP would introduce a new regulatory site that may enhance alternative splicing (RegRNA) and an exon identity element analysis predicted disruption of a silencing element (HSF). The rs36144485

variation is a 4 bp deletion (TGTT) that is predicted to disrupt silencing motifs IIE (intron identity elements) sites. The rs208307 wild-type subject was wild-type at each of these SNPs, however heterozygote at rs17526121 in intron 6 that is predicted to disrupt a potential branch-point site (HSF).

To determine if the 7 variants identified in introns 6 and 7 are inherited as a haplotype block tagged by rs208307, a further 8 subjects were genotyped (Table 3) and pairwise linkage disequilibrium (LD) was calculated using PLINK (http://pngu.mgh.harvard.edu/purcell/plink/) (31). Complete LD was found between rs36144485, rs208307, rs208308, rs208309 and rs373655596 ($r^2 = 1$); and rs208306 was in high LD with each of these 5 SNPs ($r^2 = 0.8$).

Homomeric P2X7L complexes are expressed on the cell surface membrane

To study protein expression of EX7_EX8del alternatively spliced mRNAs, P2X7A (PJB3), P2X7E and P2X7L EE-labelled constructs were transfected into HEK 293 cells. Whole-cell lysates of transfected cells were analysed by Western blot and probed using anti-EE. Proteins were detected at ~68, 31 and 58 kDa (Fig. 4A, lanes 2, 3, and 4) which corresponded to the expected molecular weights (MW) of P2X7A, P2X7E, and P2X7L, respectively. To study cell surface expression of EX7_EX8del alternatively spliced protein isoforms, HEK 293 cells were transiently transfected with P2X7A, E or L and analysed by flow cytometry after labelling with extracellular anti-P2X7 polyclonal antibody (pAb) APR008 raised against amino acids 136-152 of P2X7A and encoded by exons 4 and 5 (Fig. 4B, top panels). Surface expression of P2X7A and P2X7L, but not P2X7E was observed. Lack of surface expression of P2X7E is consistent with absence of the C terminal that contains key structural motifs required for cell surface localization (34, 35). P2X7 surface expression was also analysed using the L4 mAb that binds to an epitope around Arg307 and inhibits receptor function (36). L4 binding was detected on the surface of P2X7A transfected HEK 293 cells, however no binding was detected in P2X7E or P2X7L transfected cells (Fig. 4B, bottom panels).

To determine if P2X7L protein isoforms interact on the surface membrane, HEK 293 cells were transiently transfected with EE-tagged P2X7A or P2X7L expression constructs. Proteins on the cell surface were crosslinked by treatment with BS3, a membrane impermeable non-cleavable protein crosslinker (Fig. 4C). For BS3-treated P2X7A-transfected cells, bands at > 160kDa, ~130 kDa and ~70 kDa, corresponding to trimers, dimers and monomers respectively, were detected by Western blotting (Fig. 4C, lane 2). For BS3-treated P2X7L-transfected cells, bands at ~ 110 kDa and ~55 kDa were detected (Fig. 4C, lane 4), which corresponded to the expected MWs of dimers and monomers respectively. Although dimers of P2X7L crosslinked at the cell surface were identified, P2X7L trimers were not detected (Fig. 4C, lane 4).

Heteromeric P2X7L and P2X7A complexes are expressed in the cell cytoplasm and surface membrane

Nickel affinity chromatography was used to determine if P2X7A and P2X7L form heteromeric complexes in the cell cytoplasm. HEK 293 cells were stably transfected with P2X7A-His and P2X7L-EE expression constructs or P2X7L-EE alone. EZview His-Select beads were used to pull down proteins interacting with P2X7A-His from whole-cell lysates in the presence of 10 mM imidazole. Samples of the whole-cell lysates and the bead eluates were separated by SDS-PAGE and Western blot was performed using near infrared immunoblotting (Fig. 5A). When expressed together in the same cell line, P2X7L-EE co-eluted with P2X7A-His (Fig. 5A, lane 4), but when expressed alone, P2X7L-EE was only detected at residual levels in the bead eluate (Fig 5A, lane 3) indicating that P2X7A and P2X7L interact in a heteromeric complex.

A Duolink proximity ligation assay (PLA) was used to validate the observation that P2X7L interacts with P2X7A. Non-transfected HEK 293 cells or cells stably transfected with P2X7L-EE or P2X7A-EE were transiently transfected with P2X7A-AcGFP and a PLA was performed. All three cell lines were successfully transfected with P2X7A-AcGFP (green fluorescence, Fig. 5B, upper row). Positive PLA signals were detected in both P2X7A-EE and P2X7L-EE stable cell lines (red fluorescence, Fig. 5B, middle row), but not in HEK 293 cells, indicating that P2X7L-EE may form a heteromeric complex with P2X7A-AcGFP.

To determine if P2X7A and P2X7L form heterotrimers in the cell surface membrane, HEK 293 cells stably transfected with P2X7A-His and P2X7L-EE or P2X7L-EE alone were treated with DTSSP, a membrane impermeable crosslinker. Nickel affinity chromatography was used to purify receptor complexes containing P2X7A-His from whole-cell lysates in the presence of 12.5 mM imidazole. Bead eluates and whole-cell lysates were separated by non-reducing SDS-PAGE and near infrared immunoblotting Western blots were performed. The presence of P2X7L alone or P2X7L and P2X7A in whole-cell lysates was confirmed by probing duplicate blots with anti-EE to detect P2X7L-EE (Fig. 6A lanes 1 and 2, between 50 and 60 kDa) or with anti-P2X7 antibody (APR008) that detects both P2X7A-His (Fig. 6A lane 4, between 60 and 80 kDa) and P2X7L-EE (Fig. 6A Lanes 3 and 4 between 50 and 60KDa). Although the absence of DTT has resulted in a diffuse banding pattern, faint bands at ~110kDa and ~170kDa corresponding to the predicted MW of P2X7L dimers and trimers, respectively, were detected in whole-cell lysates of cells expressing P2X7L alone (Fig. 6A lane 3) and less distinctly in the other lanes. As observed previously (Fig. 5), small amounts of P2X7L-EE were eluted from whole-cell lysates using the His select beads (Fig. 6A, lanes 1 and 3). Probing blots with anti-EE and anti-P2X7 detected a band at ~170 kDa corresponding to the predicted MW of a P2X7L-EE homotrimer (Fig. 6B lane, 1 and 3, bold arrows).

Three distinct bands corresponding to the MWs of P2X7A-His monomers, dimers and trimers were detected in bead eluates of doubly transfected cells probed with anti-P2X7 (Fig. 6B, lane 4), but not with anti-EE (Fig. 6B lane 2). A Western blot of bead eluates from doubly transfected cells probed with anti-EE (Fig. 6B lane 2, chevron arrow) detected a complex that migrated midway between the position of the P2X7A dimer (A2, ~160kD) and trimer (A3,~260kD, Fig. 6B lane 4) and slightly behind the P2X7L trimer faintly detectable at ~170kDa (Fig. 6B lanes 1 and 3), consistent with formation of a heterotrimer of P2X7A-His and P2X7L-EE. At the corresponding position on the blot probed with anti-P2X7 (Fig 6B, lane 4) only a dark smear rather than a distinct band was observed. Heterotrimerization and/or cell surface crosslinking may have obscured the anti-P2X7 binding site as it is located in the extracellular domain but not the anti-EE epitope which is located on the intracellular C terminus of P2X7L-EE. The doublet observed in Fig. 6B. (lanes 1 and 2 at approximately 110kDa) is likely to correspond to endogenous HEK293 proteins with naturally occurring EE and His epitopes.

P2X7L has phagocytic but not channel or pore function

To determine whether EX7_EX8del protein isoforms form functional receptors, patch-clamping and Ca^{+} flux was used to measure channel function, and ethidium^{+} uptake measured by time resolved flow cytometry was used to analyse pore function in HEK 293 cells transiently transfected with either P2X7A, P2X7L or P2X7E. In addition, phagocytic function, in the absence of ATP, was analyzed by measuring the uptake of YG beads using flow cytometry (8, 9, 37). Channel and

pore function were not detected in either P2X7E or P2X7L transfected cells (Fig. 7A, B and C), however P2X7L showed the same level of phagocytic function compared to P2X7A (Fig. 7D). P2X7E, which is not trafficked to the cell surface, failed to confer phagocytic function (Fig. 7D).

P2X7 receptor pore function is altered following double-transfection of P2X7A and P2X7L

Since co-assembly of P2X7A with the C-terminus deleted P2X7B protein isoform potentiates P2X7 pore function (19), ethidium$^+$ uptake was studied in HEK 293 cells that had been double-transfected with P2X7A and either P2X7E or P2X7L. P2X7A was co-transfected with equal amounts of P2X7E or P2X7L (1 µg total plasmid DNA) and cells transfected with single plasmids were included as controls. Pore function was measured by ATP-induced ethidium$^+$ uptake using a plate reader-based assay. Confirming earlier observations using time resolved flow cytometry (Fig 7C), single transfections of P2X7L and P2X7E showed no ethidium$^+$ uptake. Pore function was unchanged following co-transfection of P2X7A and P2X7E, however, co-transfection of P2X7A and P2X7L reduced the rate of ethidium$^+$ uptake by ~50% (Fig. 8, $p < 0.0001$). Cell surface expression of P2X7A and P2X7E or P2X7L could not be measured by flow cytometry as currently there are no antibodies that differentiate P2X7A from EX7_EX8del protein isoforms. Expression of protein isoforms was inferred from plasmid-derived mRNA expression in transfected cell populations using primer sets 4 (mRNA derived from P2X7A and P2X7L plasmids) and 9 (mRNA from P2X7E and P2X7L plasmids; Table 1). Cells double-transfected with P2X7A and P2X7E showed similar levels of mRNA expression determined by sets 4 and 9. Similarly, approximately equal amounts of P2X7A and P2X7L mRNAs were expressed, with P2X7A + P2X7L mRNAs measured by set 4 expected to be double expression of P2X7L measured by set 9 (Table S1).

DISCUSSION

In this paper, we report cloning and expression of a novel *P2RX7* splice variant, *P2RX7L,* which is characterized by skipping of exons 7 and 8. A six SNP haplotype was found to induce partial allele specific alternative splicing, increasing mRNA levels of EX7_EX8del splice variants. Deletion of exons 7 and 8 will excise asparagine 292 and arginine 294 residues, both of which are predicted to interact with ATP in the ligand-binding site of human P2X7 (38). Significantly, P2X7L was found to form a heteromeric complex when co-expressed with P2X7A. In transfected HEK 293 cells, P2X7L showed phagocytic, but not channel or pore function. Compared to P2X7A alone, double-transfection of P2X7L and P2X7A reduced pore function by ~50%.

P2RX7 mRNA isoforms were studied in human PBMCs using a novel method that combined qualitative RT-PCR and qRT-PCR. For qualitative RT-PCR, three primer sets (Table 1, sets 1-3) were designed to distinguish between splice isoforms based on amplicon size whereas for qRT-PCR, *P2RX7* specific primers were designed to target sites of either intron-retention, exon-skipping or alternative exon insertion (Table 1, set 4-9). In contrast to the qualitative primer sets, quantitative primer sets were designed to detect a single splicing feature, generate small amplicons to ensure amplification efficiency, and where possible span exon-exon boundaries. Considerable inter-individual variation was observed in both qualitative and quantitative analyses particularly with respect to Ex7_Ex8del mRNA levels (Fig. 1A and B). This finding was significant considering EX7_EX8del is predicted to excise the P2X7 ATP-binding site based on mutagenesis studies and the crystal structure of zP2X4 (38, 39).

Participant genotypes were examined, and an association was found between low or absent EX7_EX8del and the minor allele at rs208307 (641-5C > G) that is located at an acceptor splice site in intron 6. In contrast, the highest levels of EX7_EX8del mRNAs were found in rs208307 homozygote minor allele subjects (Table 2). EX7_EX8del mRNA transcript levels correlated with allele-dosage of rs208307, with the highest levels in homozygote, intermediate in heterozygote, and lowest in wildtype (Fig.3A). However, it is likely that other pre-mRNA processing events regulate skipping of exons 7 and 8, as rs208307 homozygote minor allele participants continue to express mRNA isoforms that retain exons 7 and 8. Furthermore, some subjects homozygote wild-type at rs208307 also expressed EX7_EX8del mRNAs at low levels. These results are consistent with partial allele-specific alternative splicing that was confirmed using an exon trapping system by cloning DNA fragments encompassing *P2RX7* Exon 7 and flanking intronic sequence into an pSPL3 trapping vector. The haplotype tagged by rs208307 (minor alleles at rs208307, rs208306, rs36144845, rs208308, rs208309 and rs373655596) demonstrated partial allele specific alternative splicing by generating transcripts both with and without inclusion of Exon 7 (Fig. 3C). Similar to other genes (40), we have shown that *P2RX7* undergoes allele-specific alternative splicing, and that inheritance contributes to differences in relative abundances of EX7_EX8del mRNAs. However, multiple factors regulate alternative splicing including cell type-specific and physiological mechanisms (41), for example, expression of P2X7B is increased in B lymphocytes following stimulation with phytohemagglutinin (19).

Alternative splicing has been shown to produce eleven human *P2RX7* mRNA isoforms, however only two truncated protein isoforms, P2X7B and P2X7J, have previously been studied at the protein level (18-21, 42). *P2RX7B* retains intron

10, which introduces a new stop codon and encodes a truncated protein lacking the last 171 aa and containing an alternate 18 aa after TM2 (19). P2X7B forms a heterotrimer with P2X7A when exogenously expressed in *Xenopus laevis* oocytes and increases receptor functions when co-transfected with P2X7A in HEK 293 cells (19). P2X7J lacks the entire intracellular C-terminus, TM2, and the distal third of the extracellular loop (20, 42). In HEK 293 cells, P2X7J also forms a heterotrimeric complex with P2X7A, however, P2X7 functions are inhibited in co-transfected Madin-Darby canine kidney cells (43). In the present study, a novel EX7_EX8del isoform, *P2RX7L*, was identified after mRNA sequences were cloned from subjects that expressed relatively high levels of EX7_EX8del mRNA isoforms. In contrast to a previously identified EX7_EX8del isoform, *P2RX7E*, it was predicted that *P2RX7L* would retain the long intracellular C-terminus including key structural motifs required for cell surface localization (34, 35). In HEK 293 cells, both *P2RX7E* and *P2RX7L*, were translated into P2X7E and P2X7L protein isoforms, respectively (Fig. 4A), but only P2X7L was expressed on the cell surface (Fig. 4B). Lack of surface expression of P2X7E is consistent with previous studies that show the long C-terminus is required for membrane trafficking and localisation (34, 44). P2X7B, which has the same alternative C-terminus as P2X7E, has previously been shown to inefficiently traffic to the cell surface (45). In singly transfected cells P2X7L formed homotrimers (Fig. 6A, lane 3), and in double transfected cells co-assembled with P2X7A to form heterotrimers (Fig 6B, lane 2). It is of interest that the P2X7 L4 mAb bound to P2X7A and not to P2X7L (Fig. 6B), which would be consistent with loss of the L4 epitope around Arg307 resulting from skipping of exons 7 and 8.

There is considerable inter-individual variation in P2X7 receptor function, including channel gating, ion sensitivity and ligand binding (24, 46). This variation has been largely attributed to inheritance of amino acid-altering non-synonymous SNPs (2). However, the present study shows that partial allele-specific alternative splicing may potentially affect receptor function by altering the proportional of fully functional P2X7A homotrimers expressed at the cell surface through the formation of heteromers. Double-expression of P2X7A and P2X7L in a cell model reduced receptor pore function by ~50%, and a previous study in 200 healthy human subjects found rs208307, labelled as “IVS6 TTTG-17TTTGTTTG” in Denlinger *et al.* (23), and rs36144845 (IVS6 G-5C), were present in those with low pore function who were wild-type at the rs3751143 (A1513C) loss-of-function SNP (23).

The recognition that partial allele-specific alternative splicing produces functional P2X7 protein isoforms that alter receptor function adds complexity to the design and interpretation of *P2RX7* genetic association studies. Most studies of *P2RX7* and disease have focused on non-synonymous SNPs that alter protein sequence; however, this present study has found intronic SNPs that contribute to variation of protein sequence between individuals and an examination of rs208307 allele frequencies in previous candidate-gene and disease association studies may be considered in light of the phenotypic consequences of allele-specific alternative splicing (40).

The consequences of allele- and tissue- specific alternative splicing on P2X7 protein isoform expression have important practical applications for P2X7 as a pharmacological target. The presence of tissue-specific isoforms may aid the design of drugs with specific actions on given P2X7-dependent physiological processes. Furthermore, an understanding of alternative splicing is required for emerging RNA therapies that use RNA interference methods to silence specific mRNA isoforms.

In conclusion, we have identified a component of the genetic regulation of *P2RX7E* and *P2RX7L* mRNA levels in native human cells and found that the P2X7L protein isoforms alters pore and phagocytic function in a cell model. Although a previous study found a potential association between rs208307 and rs36144845 and low pore function in human subjects (23), further studies are required to fully characterize the effects of P2X7L on receptor function. At present, studies are limited by the absence of antibodies that differentiate EX7_EX8del protein isoforms from P2X7A, however advances in proteomic techniques are expected to provide a better understanding of P2X7 receptor structure and function resulting from alternative splicing.

ACKNOWLEDGEMENTS

This research was funded by a 2011 NMRF Grant.

Dr Robert Formosa, DNA Laboratory, Faculty of Health Sciences, University of Malta, Malta who donated the exon trapping vector.

Dr Michael Yarski, Millenium Science (Mulgrave, Australia) for use of Licor equipment and near infrared immunoblotting antibodies.

AUTHOR CONTRIBUTIONS

K.Skarratt designed and performed research and analysed data; M.Lovelace designed PLA experiments; B.Gu and L.Stokes contributed cell lines and designed experiments; C.Milligan performed electrophysiology measurements and analysed data; S.Petrou designed and supervised electrophysiology experiments; R.Glover analysed data; J.Wiley designed experiments and S.Fuller designed experiments, analysed data and wrote the paper.

REFERENCES

1. Torres, G. E., Egan, T. M., and Voigt, M. M. (1999) Hetero-oligomeric assembly of P2X receptor subunits. Specificities exist with regard to possible partners. *J Biol Chem* **274**, 6653-6659
2. Bartlett, R., Stokes, L., and Sluyter, R. (2014) The P2X7 receptor channel: recent developments and the use of P2X7 antagonists in models of disease. *Pharmacol Rev* **66**, 638-675
3. Mariathasan, S., Weiss, D. S., Newton, K., McBride, J., O'Rourke, K., Roose-Girma, M., Lee, W. P., Weinrauch, Y., Monack, D. M., and Dixit, V. M. (2006) Cryopyrin activates the inflammasome in response to toxins and ATP. *Nature* **440**, 228-232
4. Gu, B. J., and Wiley, J. S. (2006) Rapid ATP-induced release of matrix metalloproteinase 9 is mediated by the P2X7 receptor. *Blood* **107**, 4946-4953
5. Garbers, C., Janner, N., Chalaris, A., Moss, M. L., Floss, D. M., Meyer, D., Koch-Nolte, F., Rose-John, S., and Scheller, J. (2011) Species specificity of ADAM10 and ADAM17 proteins in interleukin-6 (IL-6) trans-signaling and novel role of ADAM10 in inducible IL-6 receptor shedding. *The Journal of biological chemistry* **286**, 14804-14811
6. Steinberg, T. H., Newman, A. S., Swanson, J. A., and Silverstein, S. C. (1987) ATP4- permeabilizes the plasma membrane of mouse macrophages to fluorescent dyes. *J Biol Chem* **262**, 8884-8888
7. Ferrari, D., Los, M., Bauer, M. K., Vandenabeele, P., Wesselborg, S., and Schulze-Osthoff, K. (1999) P2Z purinoreceptor ligation induces activation of caspases with distinct roles in apoptotic and necrotic alterations of cell death. *FEBS Lett* **447**, 71-75
8. Gu, B. J., Saunders, B. M., Jursik, C., and Wiley, J. S. (2010) The P2X7-nonmuscle myosin membrane complex regulates phagocytosis of nonopsonized particles and bacteria by a pathway attenuated by extracellular ATP. *Blood* **115**, 1621-1631
9. Gu, B. J., Rathsam, C., Stokes, L., McGeachie, A. B., and Wiley, J. S. (2009) Extracellular ATP dissociates nonmuscle myosin from P2X(7) complex: this dissociation regulates P2X(7) pore formation. *Am J Physiol Cell Physiol* **297**, C430-439
10. Khadra, A., Tomic, M., Yan, Z., Zemkova, H., Sherman, A., and Stojilkovic, S. S. (2013) Dual gating mechanism and function of P2X7 receptor channels. *Biophysical journal* **104**, 2612-2621
11. Trabanelli, S., Ocadlikova, D., Gulinelli, S., Curti, A., Salvestrini, V., Vieira, R. P., Idzko, M., Di Virgilio, F., Ferrari, D., and Lemoli, R. M. (2012) Extracellular ATP exerts opposite effects on activated and regulatory CD4+ T cells via purinergic P2 receptor activation. *J Immunol* **189**, 1303-1310
12. Nicke, A., Baumert, H. G., Rettinger, J., Eichele, A., Lambrecht, G., Mutschler, E., and Schmalzing, G. (1998) P2X1 and P2X3 receptors form stable trimers: a novel structural motif of ligand-gated ion channels. *Embo J* **17**, 3016-3028
13. Hattori, M., and Gouaux, E. (2012) Molecular mechanism of ATP binding and ion channel activation in P2X receptors. *Nature* **485**, 207-212
14. North, R. A. (2002) Molecular physiology of P2X receptors. *Physiol Rev* **82**, 1013-1067
15. Worthington, R. A., Smart, M. L., Gu, B. J., Williams, D. A., Petrou, S., Wiley, J. S., and Barden, J. A. (2002) Point mutations confer loss of ATP-induced human P2X(7) receptor function. *FEBS Lett* **512**, 43-46
16. Gu, B. J., Sluyter, R., Skarratt, K. K., Shemon, A. N., Dao-Ung, L. P., Fuller, S. J., Barden, J. A., Clarke, A. L., Petrou, S., and Wiley, J. S. (2004) An Arg307 to Gln polymorphism within the ATP-binding site causes loss of function of the human P2X7 receptor. *J Biol Chem* **279**, 31287-31295
17. Lander, E. S., Linton, L. M., Birren, B., Nusbaum, C., Zody, M. C., Baldwin, J., Devon, K., Dewar, K., Doyle, M., FitzHugh, W., Funke, R., Gage, D., Harris, K., Heaford, A., Howland, J., Kann, L., Lehoczky, J., LeVine, R., McEwan, P., McKernan, K., Meldrim, J., Mesirov, J. P., Miranda, C., Morris, W., Naylor, J., Raymond, C., Rosetti, M., Santos, R., Sheridan, A., Sougnez, C., Stange-Thomann, Y., Stojanovic, N., Subramanian, A., Wyman, D., Rogers, J., Sulston, J., Ainscough, R., Beck, S., Bentley, D., Burton, J., Clee, C., Carter, N., Coulson, A., Deadman, R., Deloukas, P., Dunham, A., Dunham, I., Durbin, R., French, L., Grafham, D., Gregory, S., Hubbard, T., Humphray, S., Hunt, A., Jones, M., Lloyd, C., McMurray, A., Matthews, L., Mercer, S., Milne, S., Mullikin, J. C., Mungall, A., Plumb, R., Ross, M., Shownkeen, R., Sims, S., Waterston, R. H., Wilson, R. K., Hillier, L. W., McPherson, J. D., Marra, M. A., Mardis, E. R., Fulton, L. A., Chinwalla, A. T., Pepin, K. H., Gish, W. R., Chissoe, S. L., Wendl, M. C., Delehaunty, K. D., Miner, T. L., Delehaunty, A., Kramer, J. B., Cook, L. L., Fulton, R. S., Johnson, D. L., Minx, P. J., Clifton, S. W., Hawkins, T., Branscomb, E., Predki, P., Richardson, P., Wenning, S., Slezak, T., Doggett, N., Cheng, J. F., Olsen, A., Lucas, S., Elkin, C., Uberbacher, E., Frazier, M., Gibbs, R. A., Muzny, D. M., Scherer, S. E., Bouck, J. B.,

Sodergren, E. J., Worley, K. C., Rives, C. M., Gorrell, J. H., Metzker, M. L., Naylor, S. L., Kucherlapati, R. S., Nelson, D. L., Weinstock, G. M., Sakaki, Y., Fujiyama, A., Hattori, M., Yada, T., Toyoda, A., Itoh, T., Kawagoe, C., Watanabe, H., Totoki, Y., Taylor, T., Weissenbach, J., Heilig, R., Saurin, W., Artiguenave, F., Brottier, P., Bruls, T., Pelletier, E., Robert, C., Wincker, P., Smith, D. R., Doucette-Stamm, L., Rubenfield, M., Weinstock, K., Lee, H. M., Dubois, J., Rosenthal, A., Platzer, M., Nyakatura, G., Taudien, S., Rump, A., Yang, H., Yu, J., Wang, J., Huang, G., Gu, J., Hood, L., Rowen, L., Madan, A., Qin, S., Davis, R. W., Federspiel, N. A., Abola, A. P., Proctor, M. J., Myers, R. M., Schmutz, J., Dickson, M., Grimwood, J., Cox, D. R., Olson, M. V., Kaul, R., Raymond, C., Shimizu, N., Kawasaki, K., Minoshima, S., Evans, G. A., Athanasiou, M., Schultz, R., Roe, B. A., Chen, F., Pan, H., Ramser, J., Lehrach, H., Reinhardt, R., McCombie, W. R., de la Bastide, M., Dedhia, N., Blocker, H., Hornischer, K., Nordsiek, G., Agarwala, R., Aravind, L., Bailey, J. A., Bateman, A., Batzoglou, S., Birney, E., Bork, P., Brown, D. G., Burge, C. B., Cerutti, L., Chen, H. C., Church, D., Clamp, M., Copley, R. R., Doerks, T., Eddy, S. R., Eichler, E. E., Furey, T. S., Galagan, J., Gilbert, J. G., Harmon, C., Hayashizaki, Y., Haussler, D., Hermjakob, H., Hokamp, K., Jang, W., Johnson, L. S., Jones, T. A., Kasif, S., Kaspryzk, A., Kennedy, S., Kent, W. J., Kitts, P., Koonin, E. V., Korf, I., Kulp, D., Lancet, D., Lowe, T. M., McLysaght, A., Mikkelsen, T., Moran, J. V., Mulder, N., Pollara, V. J., Ponting, C. P., Schuler, G., Schultz, J., Slater, G., Smit, A. F., Stupka, E., Szustakowki, J., Thierry-Mieg, D., Thierry-Mieg, J., Wagner, L., Wallis, J., Wheeler, R., Williams, A., Wolf, Y. I., Wolfe, K. H., Yang, S. P., Yeh, R. F., Collins, F., Guyer, M. S., Peterson, J., Felsenfeld, A., Wetterstrand, K. A., Patrinos, A., Morgan, M. J., de Jong, P., Catanese, J. J., Osoegawa, K., Shizuya, H., Choi, S., Chen, Y. J., and Szustakowki, J. (2001) Initial sequencing and analysis of the human genome. *Nature* **409**, 860-921

18. Cheewatrakoolpong, B., Gilchrest, H., Anthes, J. C., and Greenfeder, S. (2005) Identification and characterization of splice variants of the human P2X7 ATP channel. *Biochem Biophys Res Commun* **332**, 17-27
19. Adinolfi, E., Cirillo, M., Woltersdorf, R., Falzoni, S., Chiozzi, P., Pellegatti, P., Callegari, M. G., Sandona, D., Markwardt, F., Schmalzing, G., and Di Virgilio, F. (2010) Trophic activity of a naturally occurring truncated isoform of the P2X7 receptor. *FASEB J* **24**, 3393-3404
20. Feng, Y. H., Li, X., Zeng, R., and Gorodeski, G. I. (2006) Endogenously expressed truncated P2X7 receptor lacking the C-terminus is preferentially upregulated in epithelial cancer cells and fails to mediate ligand-induced pore formation and apoptosis. *Nucleosides Nucleotides Nucleic Acids* **25**, 1271-1276
21. Sun, C., Chu, J., Singh, S., and Salter, R. D. (2010) Identification and characterization of a novel variant of the human P2X(7) receptor resulting in gain of function. *Purinergic Signal.* **6**, 31-45
22. Chessell, I. P., Simon, J., Hibell, A. D., Michel, A. D., Barnard, E. A., and Humphrey, P. P. (1998) Cloning and functional characterisation of the mouse P2X7 receptor. *FEBS Lett* **439**, 26-30
23. Denlinger, L. C., Coursin, D. B., Schell, K., Angelini, G., Green, D. N., Guadarrama, A. G., Halsey, J., Prabhu, U., Hogan, K. J., and Bertics, P. J. (2006) Human P2X7 pore function predicts allele linkage disequilibrium. *Clin Chem* **52**, 995-1004
24. Fuller, S. J., Stokes, L., Skarratt, K. K., Gu, B. J., and Wiley, J. S. (2009) Genetics of the P2X7 receptor and human disease. *Purinergic Signal* **5**, 257-262
25. Skarratt, K. K., and Fuller, S. J. (2014) Quantitative real-time PCR eliminates false-positives in colony screening PCR. *Journal of Microbiological Methods* **96**, 99-100
26. Skarratt, K. K., Fuller, S. J., Sluyter, R., Dao-Ung, L. P., Gu, B. J., and Wiley, J. S. (2005) A 5' intronic splice site polymorphism leads to a null allele of the P2X7 gene in 1-2% of the Caucasian population. *FEBS Lett* **579**, 2675-2678
27. Jursik, C., Sluyter, R., Georgiou, J. G., Fuller, S. J., Wiley, J. S., and Gu, B. J. (2007) A quantitative method for routine measurement of cell surface P2X7 receptor function in leucocyte subsets by two-colour time-resolved flow cytometry. *J Immunol Methods* **325**, 67-77
28. Gu, B. J., Sun, C., Fuller, S., Skarratt, K. K., Petrou, S., and Wiley, J. S. (2014) A quantitative method for measuring innate phagocytosis by human monocytes using real-time flow cytometry. *Cytometry A* **85**, 313-321
29. Wilkinson, S. M., Barron, M. L., O'Brien-Brown, J., Janssen, B., Stokes, L., Werry, E. L., Chishty, M., Skarratt, K. K., Ong, J. A., Hibbs, D. E., Vugts, D. J., Fuller, S., Windhorst, A. D., and Kassiou, M. (2017) Pharmacological Evaluation of Novel Bioisosteres of an Adamantanyl Benzamide P2X7 Receptor Antagonist. *ACS chemical neuroscience* **8**, 2374-2380
30. Gu, B. J., and Wiley, J. S. (2012) Broad Applications of Multi-Colour Time-resolved Flow Cytometry. In *Flow Cytometry- Recent Perspectives* (Schmid, I., ed) pp. 185-202, InTech Open

31. Purcell, S., Neale, B., Todd-Brown, K., Thomas, L., Ferreira, M. A., Bender, D., Maller, J., Sklar, P., de Bakker, P. I., Daly, M. J., and Sham, P. C. (2007) PLINK: a tool set for whole-genome association and population-based linkage analyses. *Am J Hum Genet* **81**, 559-575
32. Desmet, F. O., Hamroun, D., Lalande, M., Collod-Beroud, G., Claustres, M., and Beroud, C. (2009) Human Splicing Finder: an online bioinformatics tool to predict splicing signals. *Nucleic Acids Res* **37**, e67
33. Huang, H. Y., Chien, C. H., Jen, K. H., and Huang, H. D. (2006) RegRNA: an integrated web server for identifying regulatory RNA motifs and elements. *Nucleic Acids Res* **34**, W429-434
34. Smart, M. L., Gu, B., Panchal, R. G., Wiley, J., Cromer, B., Williams, D. A., and Petrou, S. (2003) P2X7 receptor cell surface expression and cytolytic pore formation are regulated by a distal C-terminal region. *J Biol Chem* **278**, 8853-8860
35. Denlinger, L. C., Sommer, J. A., Parker, K., Gudipaty, L., Fisette, P. L., Watters, J. W., Proctor, R. A., Dubyak, G. R., and Bertics, P. J. (2003) Mutation of a dibasic amino acid motif within the C terminus of the P2X7 nucleotide receptor results in trafficking defects and impaired function. *J Immunol* **171**, 1304-1311
36. Buell, G., Chessell, I. P., Michel, A. D., Collo, G., Salazzo, M., Herren, S., Gretener, D., Grahames, C., Kaur, R., Kosco-Vilbois, M. H., and Humphrey, P. P. (1998) Blockade of human P2X7 receptor function with a monoclonal antibody. *Blood* **92**, 3521-3528
37. Leeson, H. C., Chan-Ling, T., Lovelace, M. D., Brownlie, J. D., Weible, M. W., 2nd, and Gu, B. J. (2019) Real-time Live-cell Flow Cytometry to Investigate Calcium Influx, Pore Formation, and Phagocytosis by P2X7 Receptors in Adult Neural Progenitor Cells. *J Vis Exp*
38. Kawate, T., Michel, J. C., Birdsong, W. T., and Gouaux, E. (2009) Crystal structure of the ATP-gated P2X(4) ion channel in the closed state. *Nature* **460**, 592-598
39. Evans, R. J. (2010) Structural interpretation of P2X receptor mutagenesis studies on drug action. *Br J Pharmacol* **161**, 961-971
40. Nembaware, V., Wolfe, K. H., Bettoni, F., Kelso, J., and Seoighe, C. (2004) Allele-specific transcript isoforms in human. *FEBS Lett* **577**, 233-238
41. Lee, Y., and Rio, D. C. (2015) Mechanisms and Regulation of Alternative Pre-mRNA Splicing. *Annual review of biochemistry* **84**, 291-323
42. Mankus, C., Rich, C., Minns, M., and Trinkaus-Randall, V. (2011) Corneal epithelium expresses a variant of P2X(7) receptor in health and disease. *PLoS One* **6**, e28541
43. Feng, Y. H., Li, X., Wang, L., Zhou, L., and Gorodeski, G. I. (2006) A truncated P2X7 receptor variant (P2X7-j) endogenously expressed in cervical cancer cells antagonizes the full-length P2X7 receptor through hetero-oligomerization. *J Biol Chem* **281**, 17228-17237
44. Wiley, J. S., Dao-Ung, L. P., Li, C., Shemon, A. N., Gu, B. J., Smart, M. L., Fuller, S. J., Barden, J. A., Petrou, S., and Sluyter, R. (2003) An Ile-568 to Asn polymorphism prevents normal trafficking and function of the human P2X7 receptor. *J Biol Chem* **278**, 17108-17113
45. Masin, M., Young, C., Lim, K., Barnes, S. J., Xu, X. J., Marschall, V., Brutkowski, W., Mooney, E. R., Gorecki, D. C., and Murrell-Lagnado, R. (2012) Expression, assembly and function of novel C-terminal truncated variants of the mouse P2X7 receptor: re-evaluation of P2X7 knockouts. *Br J Pharmacol* **165**, 978-993
46. Stokes, L., Fuller, S. J., Sluyter, R., Skarratt, K. K., Gu, B. J., and Wiley, J. S. (2010) Two haplotypes of the P2X(7) receptor containing the Ala-348 to Thr polymorphism exhibit a gain-of-function effect and enhanced interleukin-1beta secretion. *The FASEB journal : official publication of the Federation of American Societies for Experimental Biology* **24**, 2916-2927

FIGURE LEGENDS

Figure 1: Qualitative and Quantitative Expression patterns of *P2RX7* mRNA isoforms in PBMCs

Primer sets 1-3, described in Table 1A, were used to qualitatively assess inter-individual differences in *P2RX7* mRNA isoform expression in PBMCs from human subjects (n = 22) by agarose gel electrophoresis of RT-PCR products. Left panel: predicted banding patterns; centre and right panel: banding patterns from 2 representative subjects. The most commonly observed difference between subjects was the presence or absence of a 199 bp band in Subject 2 lane S3 (arrow). Panels are from the same image with irrelevant lanes cropped out. *Molecular size marker: 100 bp DNA ladder; **Negative control. B) Quantitative assessment of the abundance of *P2RX7* mRNA isoform groups relative to total *P2RX7* mRNA was made by qRT-PCR using primer sets 4-9 (Table 1B) and expressed as a percentage of total *P2RX7* mRNA in PBMCs from human subjects (n = 20).

Figure 2: Comparison of novel isoform P2X7L with P2X7A and P2X7E

Schematic representation of mRNA isoforms of *P2RX7A, E* and *L*. Exons are represented by alternating black and white rectangles. The horizontal line linking exons 10 and 11 in *P2RX7E* represents Int 10 (M: position of translation start codon; **●:** translation stop codon**).** B) Amino acid length and predicted molecular weights of P2X7A, E and L.

Figure 3: EX7_EX8del mRNA levels are associated with gene dosage at rs208307

Expression levels of **EX7_EX8del mRNA between subjects who were wild-type (n = 10), heterozygous (n = 8) or homozygous (n = 2) at rs208307. There was a difference between the 3 groups (one-way ANOVA p < 0.0001 followed by Tukey's post hoc analysis). * p = 0.0005; ** p < 0.001; *** p < 0.018. WT: wild-type; HET: heterozygote; HOM: homozygote. B) Schematic representation of the structure of the exon** trapping vector, pSPL3, containing a 494 bp fragment of *P2RX7* spanning Exon 7 from 2 subjects either WT or HOM, respectively at rs208307. MCS: multiple cloning site. C) HEK 293 Cells were transfected with one of the 2 plasmids or empty pSPL3 vector and total mRNA was isolated. RT-PCR was performed, and PCR products were resolved on a 2% agarose gel. The WT plasmid generated a 393bp mRNA fragment, while the mutant plasmid generated a 393bp fragment and a 263bp fragment identical to the empty vector. M: DNA ladder. Panels from the same image with irrelevant lanes cropped out.

Figure 4: Protein expression of P2X7L.

A) Western blot analysis of whole-cell lysates from HEK 293 cells transfected with EE-labelled P2X7A, E and L expression constructs. Whole-cell lysates were immunoblotted with anti-EE antibody. Proteins were detected at ~68, 31 and 58 kDa that corresponds to the expected molecular weights (MW) of P2X7A (solid arrow), P2X7E (chevron arrow), and P2X7L (thin arrow), respectively. Panels are from the same image with irrelevant lanes cropped out. B) Flow cytometry analyses of HEK 293 cells transiently transfected with P2X7A, E or L labelled with APR008 anti-P2X7 pAb (upper panels) or L4 mAb (lower panels). APR008 was positive for P2X7A and P2X7L, but not P2X7E. L4, which binds to an epitope located around Arg307, was positive for P2X7A, but not P2X7E or P2X7L. C) Western blot analysis of whole-cell lysates from HEK 293 cells following protein crosslinking. HEK 293 cells were transiently transfected with EE-tagged P2X7A or L expression constructs and crosslinked with BS3. Immunoblots were probed with anti-EE. Trimers, dimers and monomers of P2X7A (A^3, A^2 and A, respectively) and dimers and monomers of P2X7L (L^2 and L, respectively) were detected. Panels are from the same image with irrelevant lanes cropped out.

Figure 5: P2X7L interacts with P2X7A

A) Nickel affinity purification of P2X7A-His tagged proteins from HEK 293 cells transfected with P2X7A-His and P2X7L-EE expression constructs (L+A) or P2X7L-EE alone (L). Whole-cell lysates (left panel) and bead eluates (right panel) were separated on an 8% Tris acetate gel and NIR immunoblotting using anti-P2X7 antibody was performed. Panels are from the same image with irrelevant lanes cropped out. (B) Duolink PLA performed on cell lines stably transfected with P2X7A-EE or P2X7L-EE expression constructs and transiently transfected with P2X7A-AcGFP. Transfected cells were identified by GFP fluorescence (top panels, 2 s exposure). Duolink PLA interactions are shown in the middle panels (red fluorescence,50 ms exposure) and cell nuclei were identified by DAPI staining (bottom panels, blue fluorescence, 16.4 ms exposure). HEK 293 cells transiently transfected with P2X7A-AcGFP expression constructs alone were used as negative controls (left panels).

Figure 6: P2X7L forms heteromers with P2X7A

Nickel affinity purification of P2X7A-His tagged proteins from HEK 293 cells transfected with P2X7A-His and P2X7L-EE expression constructs (L+A) or P2X7L-EE alone (L) crosslinked at the cell surface with DTSSP. Proteins from whole-cell lysates (A) and bead eluates (B) were separated on 6% Tris-acetate gels under non-reducing conditions. NIR immunoblotting was performed on duplicate blots with anti-EE to detect P2X7L-EE

(Figure 7A and 7B, lanes 1 and 2) or with anti-P2X7 antibody to detect P2X7A-His and P2X7L-EE (Figure 7A and 7B, lanes 3 and 4). Panels are from the same image with irrelevant lanes cropped out. A, A2 and A3 indicate monomers, dimers and trimers of P2X7A-His, respectively. Bold arrows indicates the position of P2X7L-EE trimers; chevron arrow indicates the position of the P2X7L-EE/P2X7A-His heterotrimer.

Figure 7. P2X7L has phagocytic but not channel or pore function

HEK 293 cells were transfected with P2X7A, P2X7E or P2X7E. A) P2X7 channel function was determined by whole-cell patch-clamping. Curves are averaged current traces from P2X7A (n=12), P2X7E (n=9) and P2X7L (n=9) in response to ATP 1 mM. The mean and SEM are calculated (**: P<0.001). B) Typical traces of 1mM ATP-stimulated Ca^{2+} influx indicated by Fura-Red intensity over 4 min. Each interval is 2 sec. C) P2X7 pore formation as measured by ATP induced ethidium uptake was abolished in HEK 293 cells transfected with P2X7E and P2X7L isoform. D) Phagocytosis of YG beads by transfected HEK-293 cells. (**:P<0.001, n=6-7).

Figure 8. P2X7 receptor pore function is altered following co-assembly of P2X7A with P2X7L

HEK 293 cells were singly-transfected with P2X7A (A), P2X7E (E) or P2X7l (L) or double-transfected with P2X7A and P2X7E (A+E) or P2X7L (A+L). Pore function was measured as the rate of ethidium uptake using a plate reader-based assay (n = 2-7). Co-transfection with equal amounts of P2X7A and P2X7L significantly decreased the rate of ethidium uptake compared to transfection with P2X7A alone. Students t-test *p < 0.0001. NT: non-transfected cells.

Table 1: Primer sets for quantitative and qualitative assessment of *P2RX7* mRNA isoforms

Table 2: SNPs predicted to influence exon 7 and 8 skipping

[1]Wild-type; [2]Heterozygote; [3]Homozygote; [4]Mean allele frequency; [5]Fisher's exact test was used to determine differences between MAF in the two groups.

Table 3 Haplotype block associated with exon 7 and 8 skipping

WT: wild-type; HET: heterozygote; HOM: homozygote. *subjects used in exon trapping experiments

Figure S1: Novel *P2RX7* mRNA transcripts

Sequences of 5 novel *P2RX7* mRNA variants aligned to *P2RX7A* using the online MAFFT tool (https://www.ebi.ac.uk/Tools/msa/mafft/). GenBank accession numbers: *P2RX7A*, Y09561; *P2RX7L*, MK465687; *P2RX7N*, MK465688; *P2RX7O*, MK465689; *P2RX7P*, MK465690; *P2RX7Q*, MK465691.

Figure S2: Amino acid sequence of P2X7L.

The nucleotide sequence of P2X7L (Figure S1) was translated to protein using an online translation tool (https://web.expasy.org/translate/) and aligned with P2X7A(Q99572). Transmembrane regions are highlighted in grey.

Table S1. Transfection ratios of plasmid mRNAs

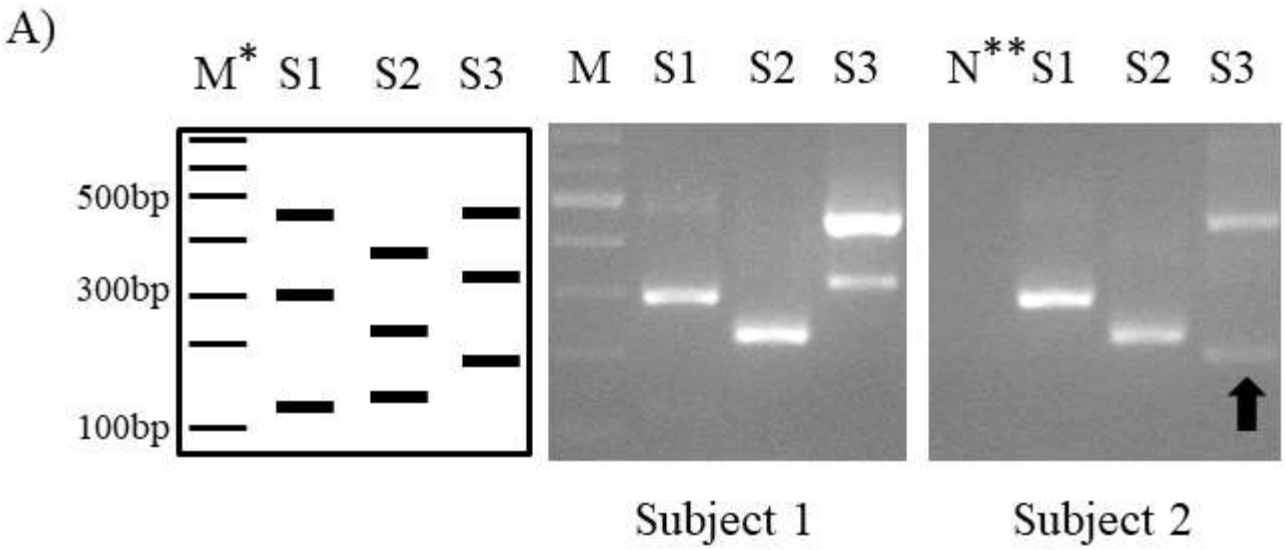
A)
M*
S1
S2
S3
M
S1
S2
S3
N**
S1
S2
S3
500bp
300bp
100bp
Subject 1
Subject 2

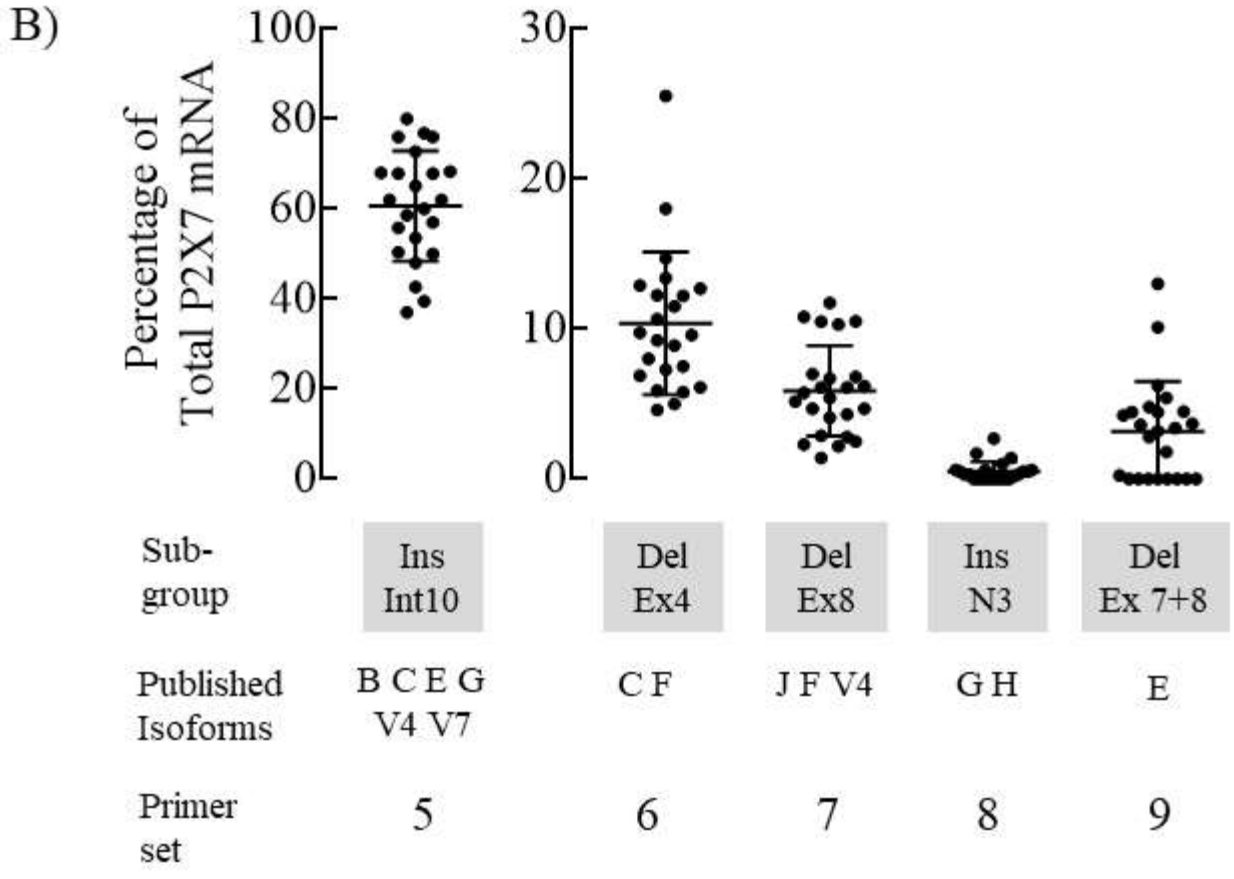
B)
Percentage of Total P2X7 mRNA
100
80
60
40
20
0
30
20
10
0
Sub-group
Ins Int10
Del Ex4
Del Ex8
Ins N3
Del Ex 7+8
Published Isoforms
B C E G V4 V7
C F
J F V4
G H
E
Primer set
5
6
7
8
9

Fig. 1

A)

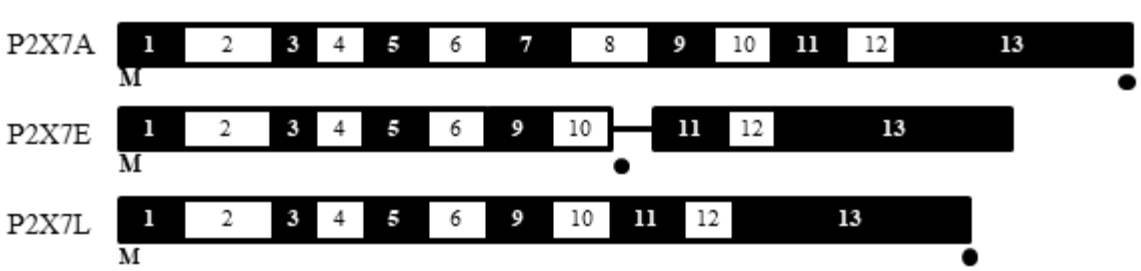

B)

Isoform	Amino Acid Length	Mol. Weight kDa
P2X7A	595	68.5
P2X7E	275	31.3
P2X7L	506	58

Figure 2

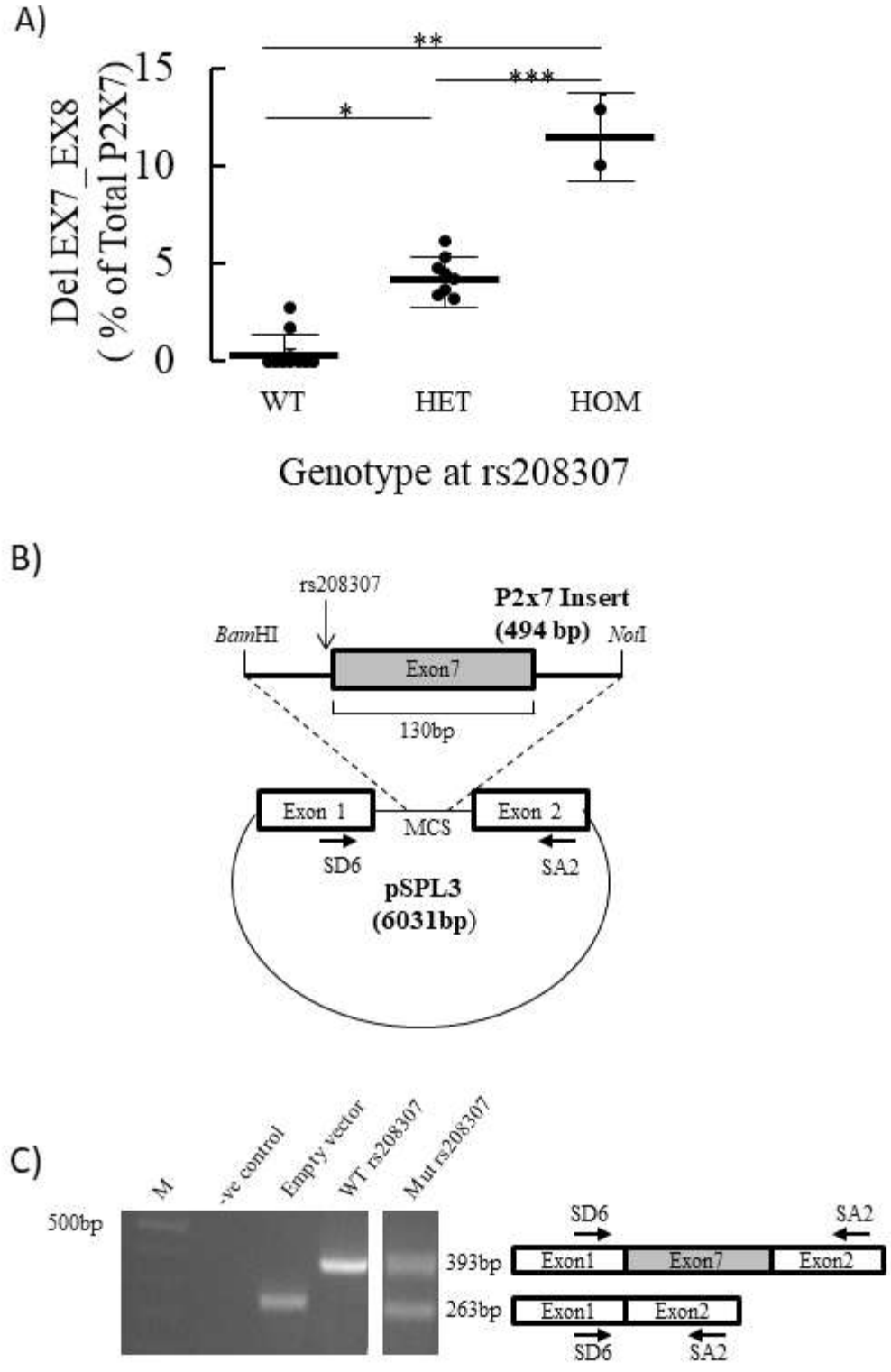
A)
Del EX7_EX8
(% of Total P2X7)
15
10
5
0
**
***
*
WT
HET
HOM
Genotype at rs208307
B)
rs208307
P2x7 Insert
(494 bp)
BamHI
NotI
Exon7
130bp
Exon 1
MCS
Exon 2
SD6
SA2
pSPL3
(6031bp)
C)
M
-ve control
Empty vector
WT rs208307
Mut rs208307
500bp
SD6
SA2
393bp
Exon1
Exon7
Exon2
263bp
Exon1
Exon2
SD6
SA2

Fig. 3

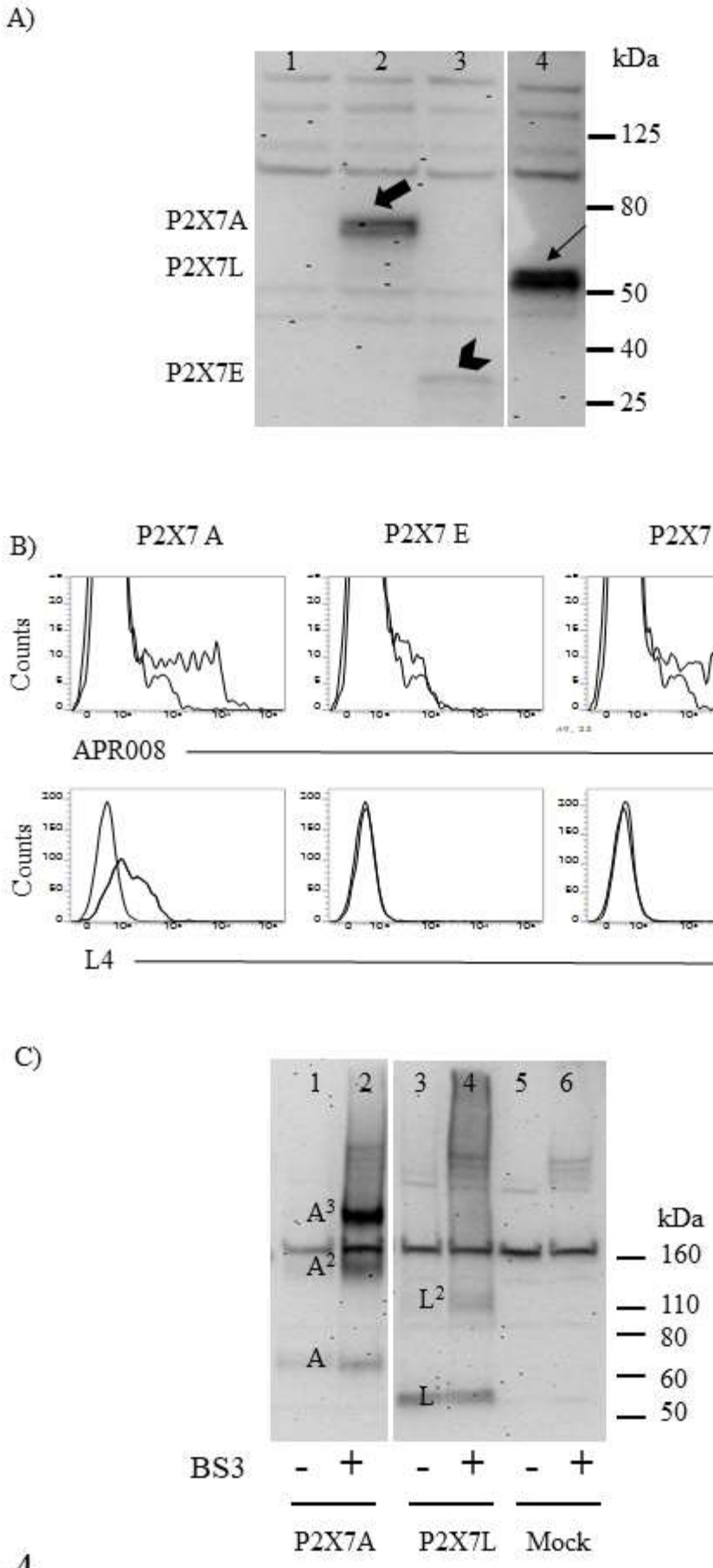
A)
1
2
3
4
kDa
125
80
50
40
25
P2X7A
P2X7L
P2X7E
B)
P2X7 A
P2X7 E
P2X7 L
Counts
APR008
Counts
L4
C)
1
2
3
4
5
6
kDa
160
110
80
60
50
A3
A2
A
L2
L
BS3
- + - + - +
P2X7A
P2X7L
Mock

Fig. 4

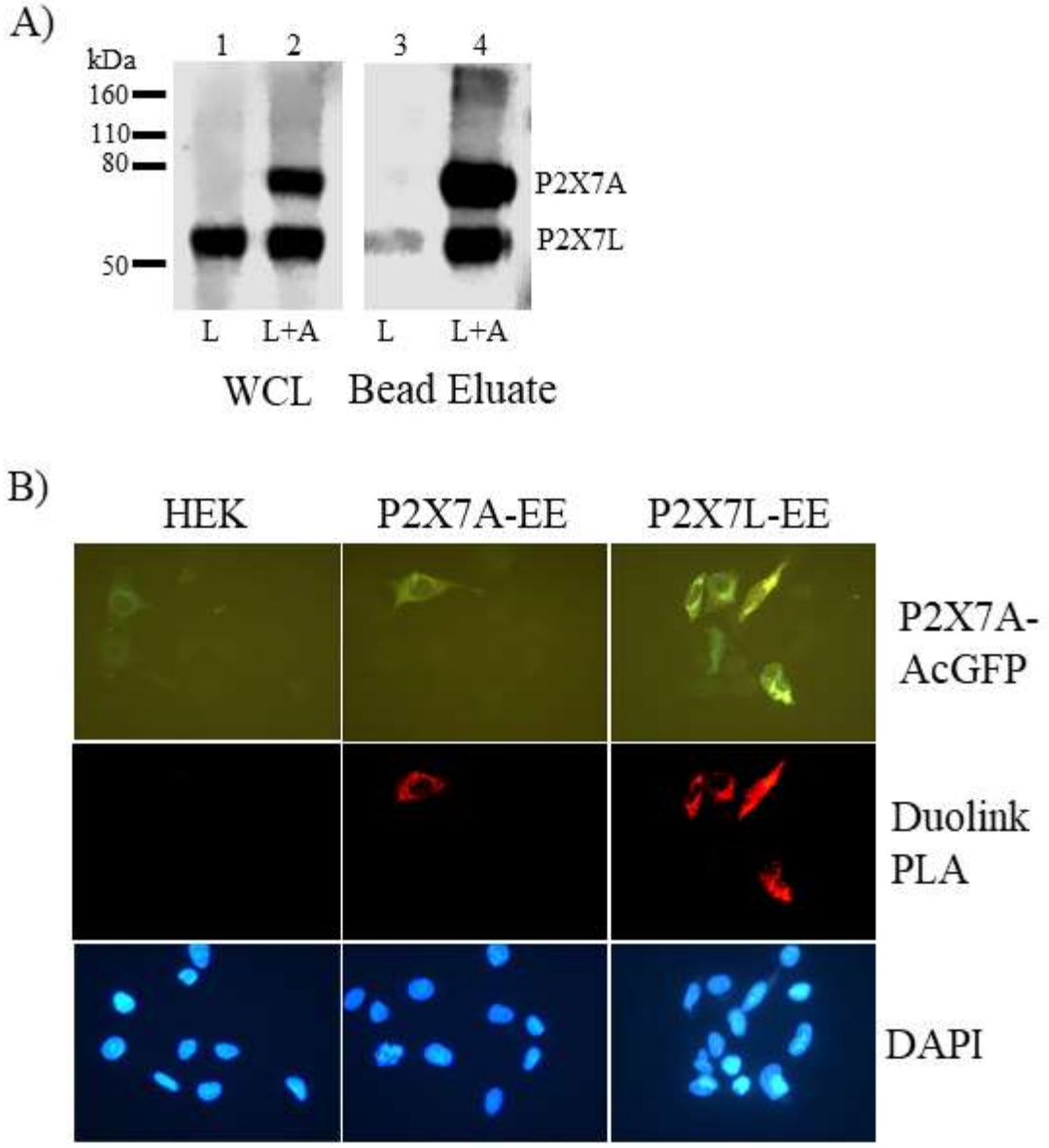
A)
kDa
160
110
80
50
1
2
3
4
P2X7A
P2X7L
L
L+A
L
L+A
WCL
Bead Eluate
B)
HEK
P2X7A-EE
P2X7L-EE
P2X7A-AcGFP
Duolink PLA
DAPI

Fig. 5

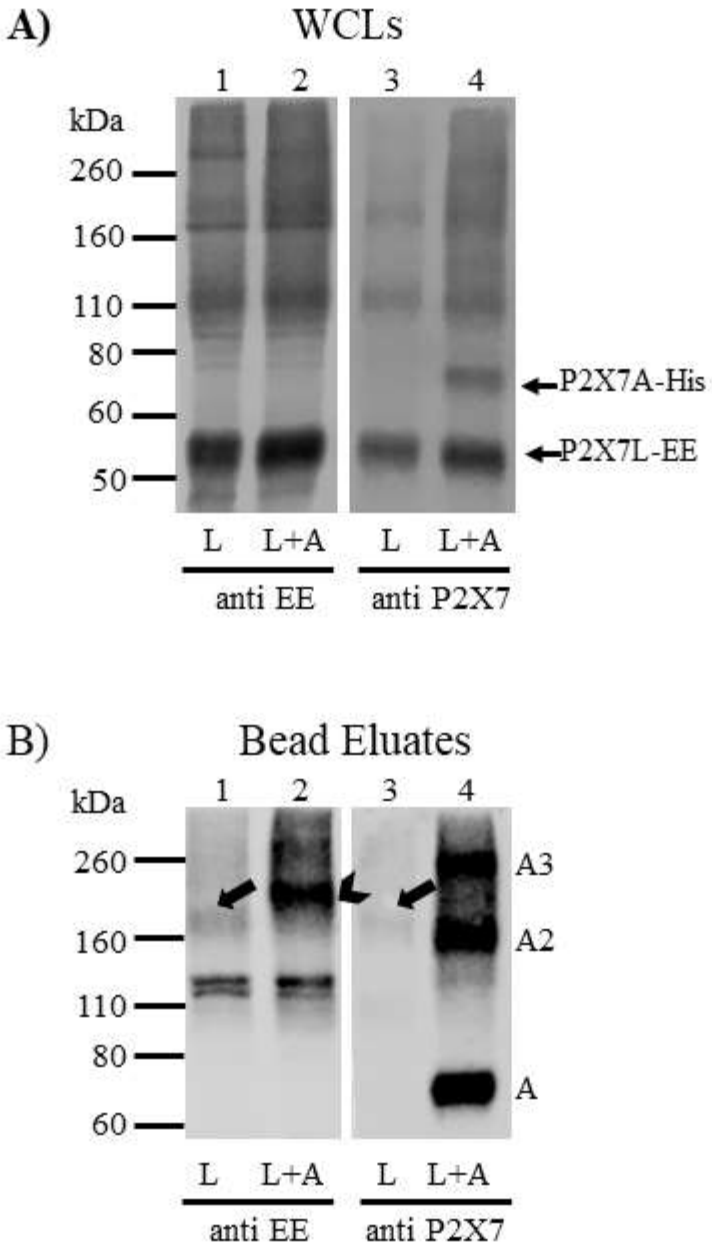
A)
WCLs
1
2
3
4
kDa
260
160
110
80
60
50
P2X7A-His
P2X7L-EE
L
L+A
L
L+A
anti EE
anti P2X7
B)
Bead Eluates
1
2
3
4
kDa
260
160
110
80
60
A3
A2
A
L
L+A
L
L+A
anti EE
anti P2X7

Figure 6

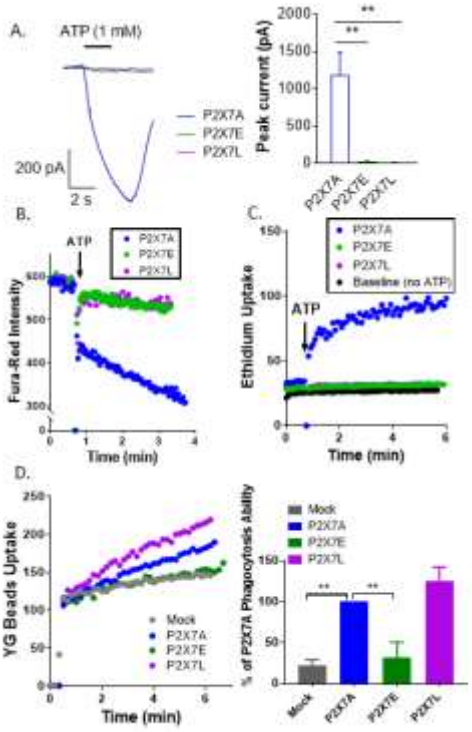
A.
ATP (1 mM)
200 pA
2 s
P2X7A
P2X7E
P2X7L
Peak current (pA)
2000
1500
1000
500
0
**
**
P2X7A
P2X7E
P2X7L
B.
ATP
P2X7A
P2X7E
P2X7L
Fura-Red Intensity
Time (min)
C.
P2X7A
P2X7E
P2X7L
Baseline (no ATP)
ATP
Ethidium Uptake
Time (min)
D.
YG Beads Uptake
Mock
P2X7A
P2X7E
P2X7L
Time (min)
% of P2X7A Phagocytosis Ability
Mock
P2X7A
P2X7E
P2X7L
**
**

Fig. 7

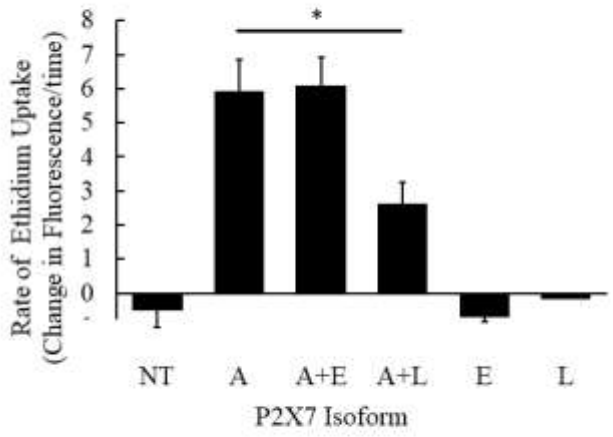
Rate of Ethidium Uptake
(Change in Fluorescence/time)
8
7
6
5
4
3
2
1
0
-
*
NT
A
A+E
A+L
E
L
P2X7 Isoform

Fig. 8

TABLES.

(A) Qualitative P2RX7 profiling

	Left primer (5'-3')	**Right primer (5'-3')**	**Product size (bp)**	***P2RX7* isoforms detected**
Set 1	ttccacgtgatcatcttttcc (in exon 1)	tcagaggaacagagcgtcct (in exon 4)	438 299 130	G H A B D E J V4 V7 ΔE2
Set 2	aaaacagaaggccaagagca (in exon 3)	tttcggcactgttcaagaga (in exon 6)	385 232 159 135	V4 A B E G H J V7 ΔE2 C F D
Set 3	tgtgaagtctctgcctggtg (in exon 5)	aacggatcccgaagactttt (in exon 9)	466 329 199	A B C G H V7 ΔE2 F J V4 E

(B) Relative Quantitative P2RX7 Profiling

	Left primer (5'-3')	**Right primer (5'-3')**	**Product size (bp)**	***P2RX7* isoforms detected**	**Isoform Group***
Set 4	ccaagaagtcccaagacctg (exon 12/13 boundary)	gtggctctcagggagttgag (in exon 13)	196	A B C D E F G H J V4 V7 ΔE2	All *P2RX7* isoforms
Set 5	aagtcttcgggatccgtttt (in exon 9)	aagcgctgcgttagtcactt (in intron 10)	174	B C E G V4 V7	Ins Intron 10
Set 6	gtgtcccgaggaattcagac (exon3/5 boundary)	aacctggcaggatgtttctc (in exon 7)	208	C F	Del Exon 4
Set 7	tttcagatgtggcaattcagata (exon 7/9 boundary)	aagtaggagagggttgagcc (in exon 10)	170	J F V4	Del Exon 8
Set 8	agaccattcttgggggaact (in exon N3)	cctcggtcagaggaacagag (in exon 4)	120	G H	Ins N3
Set 9	gccacaactacaccacatacg (exon 6/9 boundary)	gagagggttgagccgatgta (in exon10)	160	E**	Del Exons 7and 8
GAPDH	cgagatccctccaaaatcaa	ttcacacccatgacgaacat	170	N/A	

*mRNA isoform groups based on specific exon deletions or insertions: inserted intron 10 (Ins Intron 10), deletion exon 4 (Del Exon 4), deletion exon 8 (Del Exon 8), incorporation of a novel exon 3 (Ins N3), deletion exons 7 and 8 (Del Exons 7 and 8). **Novel isoform *P2RX7L* is also detected with this primer set.

Table 1

		Del Exon7+8 mRNA										
		Absent					Present					
SNP	**Location**	***n***	**WT[1]**	**HET[2]**	**HOM[3]**	**MAF[4]**	***n***	**WT**	**HET**	**HOM**	**MAF**	**p-Value[5]**
rs208307	intron 6	6	6	0	0	0	14	4	8	2	0.43	0.007
rs503720	intron 7	5	3	2	0	0.20	12	5	5	2	0.38	0.07
rs7958311	exon 8	6	1	4	1	0.50	17	16	5	0	0.15	0.02
rs7958316	exon 8	6	6	0	0	0	17	16	1	0	0.03	1.00

Table 2

		rs208307									
		WT			HET			HOM			
SNP	Location	Sub 1*	Sub 2	Sub 3	Sub 4	Sub 5	Sub 6	Sub 7	Sub 8	Sub 9	Sub 10*
rs208306	Intron 6	WT	WT	WT	HET	WT	HET	HOM	HOM	HOM	HOM
rs17526121	Intron 6	HET	WT	HET	HET	WT	WT	WT	WT	WT	WT
rs36144845	Intron 6	WT	WT	WT	HET	HET	HET	HOM	HOM	HOM	HOM
rs208308	Intron 7	WT	WT	ND	HET	HET	HET	HOM	HOM	HOM	HOM
rs208309	Intron 7	WT	WT	ND	HET	HET	HET	HOM	HOM	HOM	HOM
rs373655596	Intron 7	WT	WT	ND	ND	HET	HET	HOM	HOM	HOM	HOM

Table 3